nature portfolio

https://doi.org/10.1038/s41586-024-08080-x

Supplementary information

Carbon dioxide capture from open air using covalent organic frameworks

In the format provided by the authors and unedited

Carbon Dioxide Capture From Open Air Using Covalent Organic Frameworks

Zihui Zhou[1,2,3,4], Tianqiong Ma[1,2,3,4], Heyang Zhang[1,2,3,4], Saumil Chheda[1,2,3,4], Haozhe Li[1,2,3,4], Kaiyu Wang[1,2,3,4], Sebastian Ehrling[5], Raynald Giovine[1], Chuanshuai Li[1,2,3,4], Ali H. Alawadhi[1,2,3,4], Marwan M. Abduljawad[4], Majed O. Alawad[4], Laura Gagliardi[6], Joachim Sauer[7]*, Omar M. Yaghi[1,2,3,4]*

[1]Department of Chemistry, University of California, Berkeley, California 94720, United States.
[2]Kavli Energy NanoScience Institute, University of California, Berkeley, California 94720, United States.
[3]Bakar Institute of Digital Materials for the Planet, College of Computing, Data Science, and Society, University of California, Berkeley, California 94720, United States.
[4]KACST-UC Berkeley Center of Excellence for Nanomaterials for Clean Energy Applications, King Abdulaziz City for Science and Technology, Riyadh 11442, Saudi Arabia.
[5]3P INSTRUMENTS GmbH & Co. KG; Bitterfelder Str. 1-5, 04129 Leipzig, Germany.
[6]Department of Chemistry, Pritzker School of Molecular Engineering, and Chicago Center for Theoretical Chemistry, University of Chicago, Chicago, Illinois 60637, United States.
[7]Institut für Chemie, Humboldt-Universität zu Berlin, 10099 Berlin, Germany.
*Corresponding authors. Emails: js@chemie.hu-berlin.de (J.S.), yaghi@berkeley.edu (O.M.Y.)

Table of Contents

Section 1. Materials and Instrumentation

Chemicals

4-Toluenesulfonyl chloride (98%), 2-chloroethanamine hydrochloride (98%), 6-chloro-1-hexanol (95%), sodium hydroxide (97%), 1,2-dichlorobenzene (99%), triphenylphosphine (99%), sodium sulfate (99%) were purchased from AK Scientific. Potassium carbonate (99%) was purchased from Alfa Aesar. 1,3,5-tris(4-cyanomethylphenyl)benzene (TCPB, 98%), 3,3′-dihydroxy-4,4'-biphenyldicarboxaldehyde (97%) were purchased from Arctom Scientific. Sodium azide ($Na^{15}NN_2$, 1-^{15}N, 98%) was purchased from Cambridge Isotope Laboratories. Cesium carbonate (Cs_2CO_3, 99.99%) was purchased from Chem-Impex International. Methanol (99.8%) was purchased from Fischer Scientific. Hexane (mixture of isomers, 98.5% sum of enantiomers) was purchased from J.T.Baker. Ethyl acetate (99.5%) was purchased from Macron Fine Chemicals. Dichloromethane (DCM, 99.5%), N,N-dimethylformamide (DMF, 99.9%), 1,4-dioxane (99%), triethylamine (99%), sodium azide (99%), toluene (99.5%), acetic acid (99.7%), 1-butanol (99.9%), chloroform-d ($CDCl_3$, 99.8 atom % D) were purchased from Sigma Aldrich. All reagents and solvents were used without further purification.

Solution-state Nuclear Magnetic Resonance Spectroscopy (Solution-State NMR)

Solution-state NMR experiments were conducted at an external field B_0= 14.1 T (600 MHz for ^1H, 151 MHz for ^{13}C, and 61 MHz for ^{15}N) using a Bruker spectrometer equipped with an Avance-III console. Chemical shifts were referenced using the solvent resonances as internal standards (δ ^1H: 7.26 ppm for $CDCl_3$; δ ^{13}C: 77.16 ppm for $CDCl_3$). A polynomial baseline correction was applied to each spectrum before integration using Mestrelab MestReNova software.

Elemental Analysis

Elemental analysis was performed in the Microanalytical Laboratory of the College of Chemistry at UC Berkeley, using a Perkin Elmer 2400 Series II CHNS elemental analyzer.

Fourier-transform infrared (FT-IR) Spectra

FT-IR spectra were collected on a Bruker ALPHA Platinum ATR-FT-IR Spectrometer equipped with a single reflection diamond ATR module. Spectra were collected on the neat samples and at room temperature (around 25 °C). Spectra are plotted in transmittance (%) against the wavenumbers (cm^{-1}).

High Resolution Mass Spectra (HR-MS)

HR-MS measurements were performed by the QB3/Chemistry Mass Spectrometry Facility at UC Berkeley. Masses are reported in m/z units as the molecule ion M^+, $[M + H]^+$, $[M + Na]^+$, $[M + K]^+$, with the corresponding intensities in %.

Thermogravimetric Analyses (TGA)

TGA curves were recorded on a TA Q500 thermal analysis system under nitrogen flow, ramping at 10 °C min^{-1} from room temperature (around 25 °C) to 800 °C. Ultrahigh-purity-grade N_2 was used for all TGA measurements.

Supercritical Carbon Dioxide Dryer

The supercritical CO_2 drying was performed by Tousimis Autosamdri-931 critical point dryer. Instrument grade CO_2 (Praxair, 99.99%) was used throughout the drying process.

Scanning Electron Microscopy (SEM)

SEM images were obtained on a Zeiss XB 550 high-resolution SEM with an accelerating voltage of 1.0 kV. The samples were dispersed on conductive carbon tape, mounted on stubs, and sputter coated (Pd/Au) with a Tousimis sputter coater on top of a Bio-Rad E5400 controller.

Section 2. Synthesis of Linkers

Synthesis of 1-hexanol, 6-azido-, 1-(4-methylbenzenesulfonate)

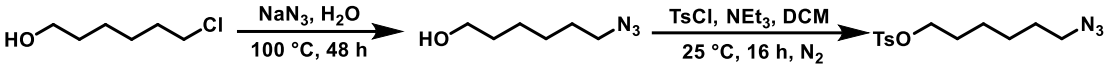

6-Chloro-1-hexanol (13.6 g, 100 mmol, 1.0 equiv.) and NaN_3 (8.5 g, 131 mmol, 1.3 equiv.) were added to 100 mL DI water and the reaction mixture was refluxed under 100 °C for 48 h. After cooling to room temperature, the mixture was extracted with ethyl acetate (100 mL × 3). The organic phase was combined, washed with water (100 mL × 3), brine (50 mL), and dried over sodium sulfate. After filtration, the solvent was evaporated to afford 6-azido-1-hexanol a colorless oil, which was used directly for the next step without further purification.

The above colorless oil was dissolved into 150 mL DCM under N_2 atmosphere, and the solution was cooled to 0 °C. 4-toluenesulfonyl chloride (21.0 g, 110 mmol, 1.1 equiv.) and triethylamine (41.8 mL, 300 mmol, 3.0 equiv.) were added to the solution. The solution was warmed to 25 °C and stirred for 16 h. 100 mL water was added upon completion, and the organic phase was collected, washed with water (100 mL) and brine (50 mL), and dried over sodium sulfate. The solution was filtered and concentrated, and the resulting oil was subjected to flash column chromatography using silica gel and with ethyl acetate/hexanes (1/5, v/v) as eluent to afford the product as a colorless oil (24.2 g, overall yield 81%). ^{1}H NMR (600 MHz, $CDCl_3$): δ (ppm) 7.79 (d, *J* = 8.4 Hz, 2H), 7.35 (d, *J* = 8.3 Hz, 2H), 4.02 (t, *J* = 6.3 Hz, 2H), 3.23 (t, *J* = 6.7 Hz, 2H), 2.45 (s, 3H), 1.65 (m, 2H), 1.54 (m, 2H), 1.33 (m, 4H).

Synthesis of 3,3'-bis[(6-azidohexyl)oxy]-4,4'-biphenyldicarbaldehyde (BPDA-N_3)

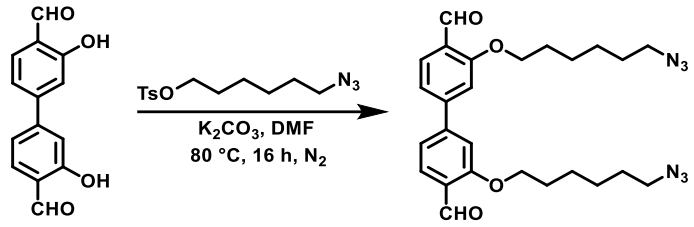

3,3′-dihydroxy-4,4'-biphenyldicarboxaldehyde (1.0 g, 4.1 mmol, 1.0 equiv.), K_2CO_3 (1.7 g, 12 mmol, 3.0 equiv.) and 1-hexanol, 6-azido-, 1-(4-methylbenzenesulfonate) (2.7 g, 9.0 mmol, 2.2 equiv.) were added to 30 mL anhydrous DMF under N_2 atmosphere. The resulting suspension was heated to 80 °C and stirred for 16 h. After cooling down, DMF was evaporated under reduced pressure, and the remaining mixture was extracted by water (100 mL) and DCM (100 mL). The organic phase was collected, washed with water (100 mL) and brine (50 mL), and dried over sodium sulfate. The solution was filtered and concentrated, and the resulting solid was subjected to flash column chromatography using silica gel and with ethyl acetate/hexanes (1/5, v/v) as eluent to afford the product as a white solid (1.52 g, yield 74%). ^{1}H NMR (600 MHz, $CDCl_3$): δ (ppm) 10.53 (s, 2H), 7.92 (d, *J* = 8.0 Hz, 2H), 7.23 (d, *J* = 8.0 Hz, 2H), 7.14 (s, 2H), 4.18 (t, *J* = 6.3 Hz,

4H), 3.30 (t, J = 6.3 Hz, 4H), 1.91 (m, 4H), 1.65 (m, 4H), 1.57 (m, 4H), 1.50 (m, 4H). ^{13}C NMR (151 MHz, $CDCl_3$) δ (ppm) 189.4, 161.8, 147.9, 129.1, 124.7, 120.0, 111.5, 68.7, 51.5, 29.1, 28.9, 26.6, 25.8. HR-ESI-MS: m/z: 515.2382 ([M + Na]$^+$, calcd. for $[C_{26}H_{32}N_6O_4Na]^+$ 515.2377).

Synthesis of aziridine

To a 500 mL round bottom flask containing sodium hydroxide aqueous solution (50.0 g NaOH in 200 mL DI water), 2-chloroethanamine hydrochloride (50.0 g, 431 mmol) was slowly added. The resultant solution was heated to 50 °C and stirred for 3 h. After the reaction, aziridine was separated by distillation at 80 °C under vacuum (20 kPa). Sodium hydroxide was added to the collected distillate for drying and the water-containing aziridine was further purified by distillation under ambient pressure (boiling point 56 °C under 101 kPa). ^{1}H NMR (600 MHz, $CDCl_3$): δ (ppm) 1.59 (s, 4H), −0.10 (s, 1H). ^{13}C NMR (151 MHz, $CDCl_3$) δ (ppm) 18.3.

Synthesis of BPDA-$^{15}N_3$

BPDA-$^{15}N_3$ was synthesized according to the method described above. ^{15}N labeled sodium azide ($Na^{15}NN_2$) was used in the reaction. BPDA-$^{15}N_3$ is a mixture of α-^{15}N (R–^{15}N=N=N) and γ-^{15}N (R–N=N=^{15}N) labeled compounds since only one of the terminal nitrogen atoms is labeled in the ^{15}N-sodium azide. ^{1}H NMR (600 MHz, $CDCl_3$): δ (ppm) 10.53 (s, 2H), 7.91 (d, J = 8.0 Hz, 2H), 7.23 (d, J = 8.0 Hz, 2H), 7.14 (s, 2H), 4.17 (t, J = 6.3 Hz, 4H), 3.30 (t, J = 6.3 Hz, 4H), 1.91 (m, 4H), 1.65 (m, 4H), 1.57 (m, 4H), 1.49 (m, 4H). ^{13}C NMR (151 MHz, $CDCl_3$): δ (ppm) 189.3, 161.8, 147.8, 129.1, 124.7, 119.9, 111.6, 68.7, 51.5 (d, J = 4.0 Hz), 29.1, 28.9, 26.6, 25.8. ^{15}N NMR (61 MHz, $CDCl_3$): δ (ppm) 210.7 (R–N=N=**^{15}N**), 71.7 (R–**^{15}N**=N=N). HR-ESI-MS: m/z: 517.2322 ([M + Na]$^+$, calcd. for $[C_{26}H_{32}N_4{}^{15}N_2O_4Na]^+$ 517.2318).

Section 3. Detailed Sorbent Comparison for Direct Air Capture

Supplementary Table 1 | Adsorption and cycling properties of selected direct air capture (DAC) sorbents.

Sorbent	Uptake (mmol g^{-1})	Adsorption Conditions				Des. Condi-tions	Cycling Stability	Ref.
		Temp. (°C)	CO_2 (ppm)	Carrier Gas	RH (%)			
Covalent organic frameworks								
COF-999	2.02	25 °C	400	N_2/O_2	50%	60 °C	10 cycles, stable	This work
	1.28[a]	Open-air				60 °C	100 cycles, stable	
COF-609	0.39	25 °C	400	N_2/O_2	50%	-	-	1
Metal-organic frameworks[2]								
SIFSIX-3-Cu	1.24[b]	25 °C	400	-	-	-	-	3
MOF-74-mmen-2	1.05[a]	25 °C	390	N_2/O_2	0%	150 °C	10 cycles, stable	4
ED-Mg/DOBDC	1.51	25 °C	400	Ar	0%	110 °C	4 cycles, stable	5
$Zn(ZnOH)_4(bibta)_3$	1.32	25 °C	395	N_2/O_2	0%	100 °C	5 cycles, stable	6
MOF-808-Lys	0.70[a]	25 °C	400	N_2/O_2	50%	140 °C	10 cycles, stable	7
Amine functionalized porous support (silica/alumina/carbon)[8]								
PEI@H-SiO_2	3.36	30 °C	400	He	19%	110 °C	5 cycles, 18% loss	9
50%TEPA@SBA-15	2.30	25 °C	400	N_2	0%	110 °C	10 cycles, 4% loss	10
PEI@$Mg_{0.55}$Al-O	2.27	25 °C	400	N_2	0%	120 °C	20 cycles, 14% loss	11
PEI@Mesoporous carbon	2.25	25 °C	400	N_2	0%	110 °C	10 cycles, 3% loss	12
Amine hybrid aerogel	1.64	30 °C	400	N_2	0%	130 °C	15 cycles, stable	13
Ph-3-ED@SBA-15	1.40[c]	35 °C	400	He	30%	90 °C	25 cycles, stable	14
PEI@SBA-15	0.96	35 °C	400	He	0%	110 °C	20 cycles, stable	15
PEI@EtSNTs	1.00	25 °C	400	N_2	0%	100 °C	8 cycles, stable	16
PEI@Alumina monolith	0.90	0 °C	400	N_2	0%	110 °C	5 cycles, 14% loss	17
PEI@Zr-SBA-15	0.85	25 °C	400	Ar	0%	110 °C	4 cycles, stable	18
PEI@Ti-SBA-15	0.64	25 °C	400	Ar	0%	110 °C	4 cycles, 6% loss	18
Polylysine@SBA-15	0.60	25 °C	400	Ar	0%	110 °C	3 cycles, stable	19
Ion-exchange resins[20] **(moisture swing adsorption)**								
HIPE templated p(NMe_3^+-MS OH^-)	0.49	18 °C	Open-air		20%	95%RH	1 cycle	21
Colloidalcrystaltemplated p(NMe_3^+-MS OH^-)	0.37	18 °C	Open-air		20%	95%RH	1 cycle	21
Amine-based anion exchange resin in polypropylene	0.98	23 °C	400	N_2/O_2	0.5%	Water	1 cycle	22
Pickering polyHIPEs	0.72	18 °C	Open-air		20%	95%RH	1 cycle	23

CO_3^{2-}-resin	0.26	20 °C	417	N_2/O_2	0%	95%RH	5 cycles, stable	24
Quaternized Chitosan/PVA Aerogels	0.18	20 °C	400	N_2	0%	95%RH	10 cycles, stable	25
Charged sorbents								
PCS-OH	0.2	30 °C	400	N_2/O_2	0%	130 °C	10 cycles, stable	26
Liquid amines								
MEA	2.46[a]	Open-air				123 °C	Amine volatilization	27
Hydroxides-carbonates								
KOH or NaOH-CaO (calcinate)	quant.	Open-air				900 °C	Stable	28

a, Not cycling under full capacity.
b, Single-component isotherm results.
c, Calculated from the weight of silica support as mmol/g_{SiO_2}.

Supplementary Table 2 | Comparison of the technical performances of different DAC technologies.[29]

Sorbent Type	Desorption/Regeneration Conditions		Regeneration Energy (GJ/tCO_2)
	Temperature (°C)	Pressure	
Hydroxides-carbonates	900 °C	Ambient	6.07 to 10.32
Liquid amines	120 to 150 °C	Ambient	11.46 to 49.08
Amine functionalized porous materials	80 to 130 °C	Vacuum	4.4 to 13.2[a]
Resins	40 to 50 °C	Water saturated air	0.65[b]
Cryogenic	–78 to –140 °C	High pressure	50 to 102

a, From the calculation (see section 12 for details), COF-999 requires a total energy of 5.89 GJ/tCO_2 for desorption under 60 °C after the adsorption from 400 ppm CO_2 and 50% RH.
b, If driven exclusively by the heat released from water condensation[20].

Section 4. Scanning Electron Microscopy (SEM)

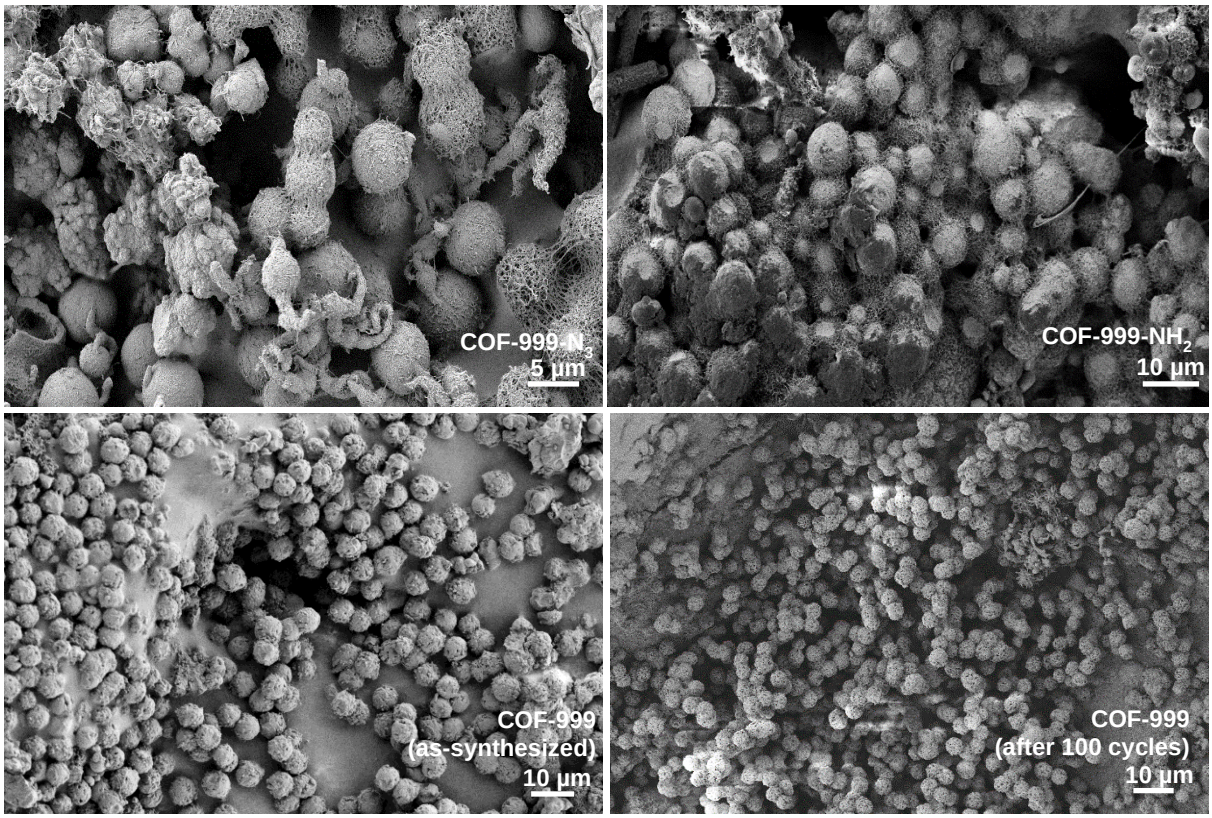

Supplementary Fig. 1 | SEM images of COF-999-N_3, COF-999-NH_2, COF-999 (as-synthesized), and COF-999 (after 100 cycles). The textured spherically shaped morphology was observed and remained unchanged during the post-synthetic modification process and the adsorption-desorption cycles.

Section 5. Single Component Sorption Measurements

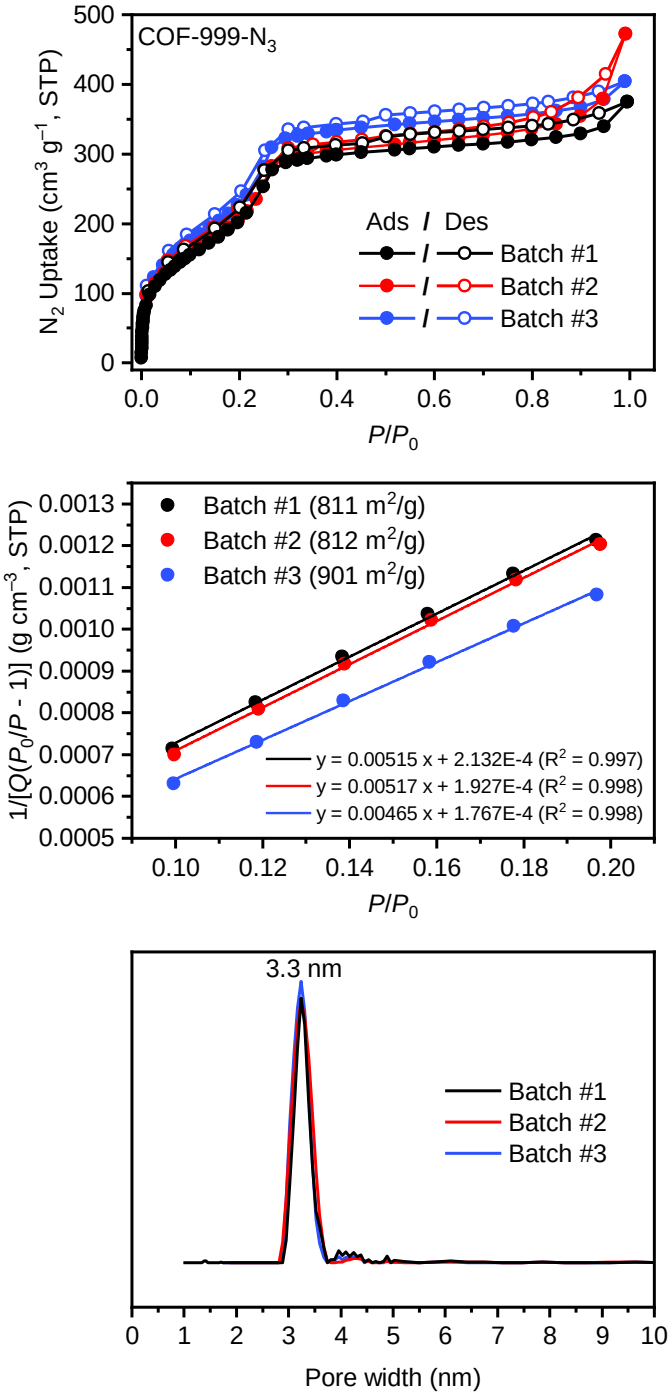

Supplementary Fig. 2 | N_2 sorption isotherms of COF-999-N_3 measured at 77 K (upper), corresponding BET plot, linear fitting (middle), and pore size distribution (lower) calculated from the sorption isotherm. Three different batches of samples were used for the measurement to show the reproducibility. The hysteresis can be attributed to the flexibility of side chains within the pores. *P*, nitrogen pressure; P_0 = 1 atm; STP, standard temperature and pressure. The isotherm for batch #1 is the same as shown in Fig. 2b in the main text.

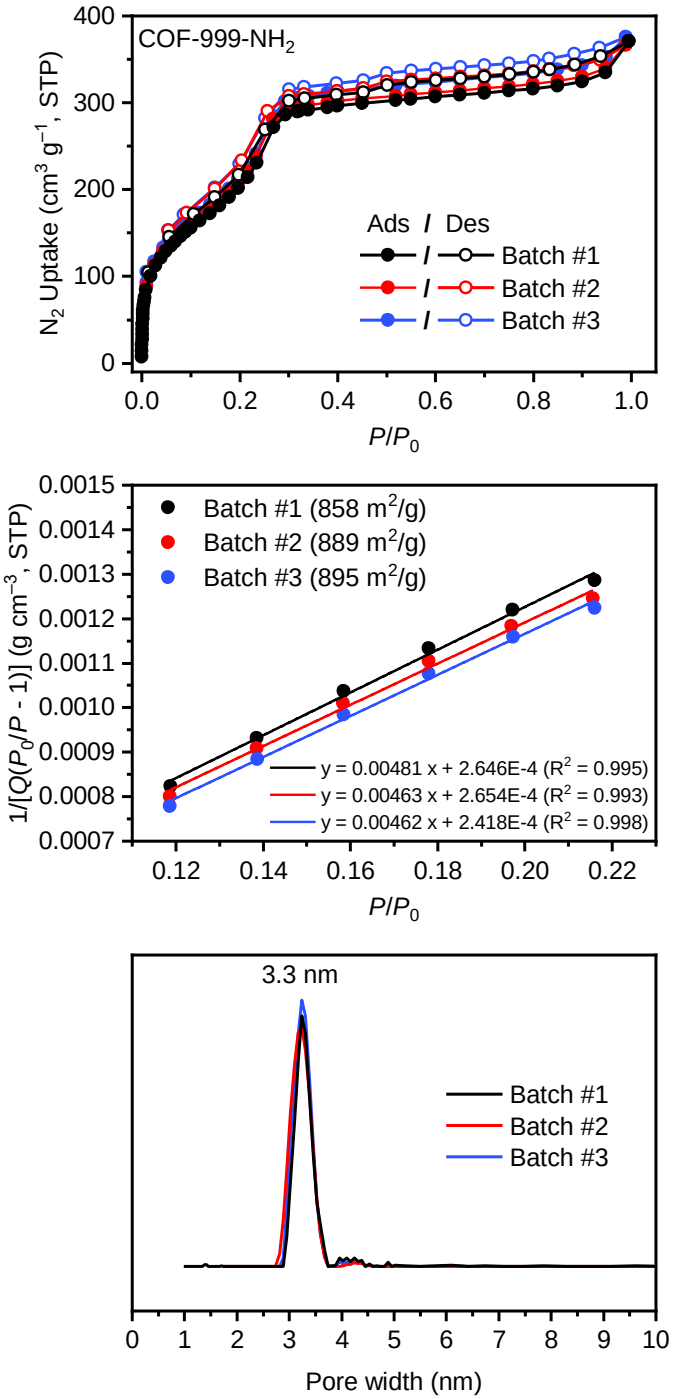

Supplementary Fig. 3 | N_2 sorption isotherms of COF-999-NH_2 measured at 77 K (upper), corresponding BET plot, linear fitting (middle), and pore size distribution (lower) calculated from the sorption isotherm. Three different batches of samples were used for the measurement to show the reproducibility. The hysteresis can be attributed to the flexibility of side chains within the pores. *P*, nitrogen pressure; P_0 = 1 atm; STP, standard temperature and pressure.

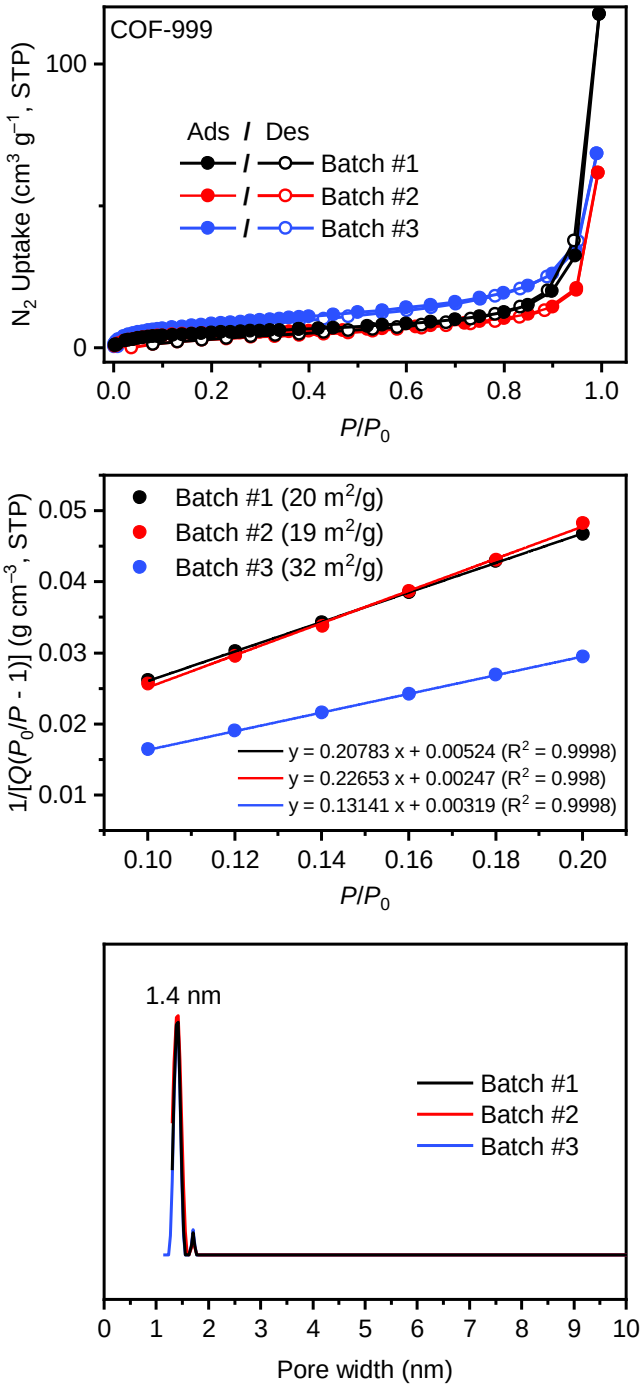

Supplementary Fig. 4 | N_2 sorption isotherms of COF-999 measured at 77 K (upper), corresponding BET plot, linear fitting (middle), and pore size distribution (lower) calculated from the sorption isotherm. Three different batches of samples were used for the measurement to show the reproducibility. The hysteresis can be attributed to the flexibility of side chains within the pores. *P*, nitrogen pressure; P_0 = 1 atm; STP, standard temperature and pressure.

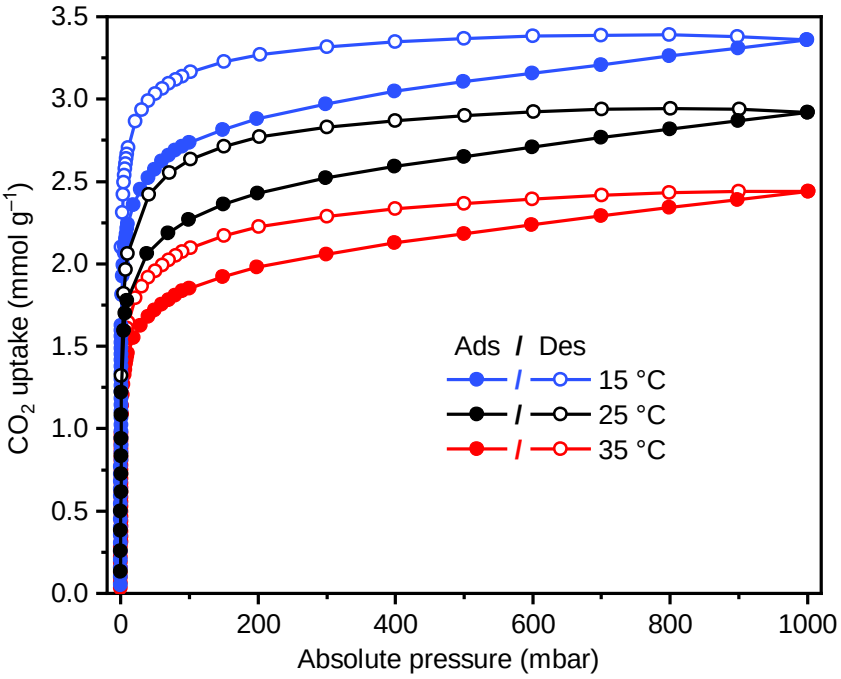

Supplementary Fig. 5 | Single-component CO_2 sorption isotherms of COF-999 measured at 15 °C (blue), 25 °C (black), and 35 °C (red).

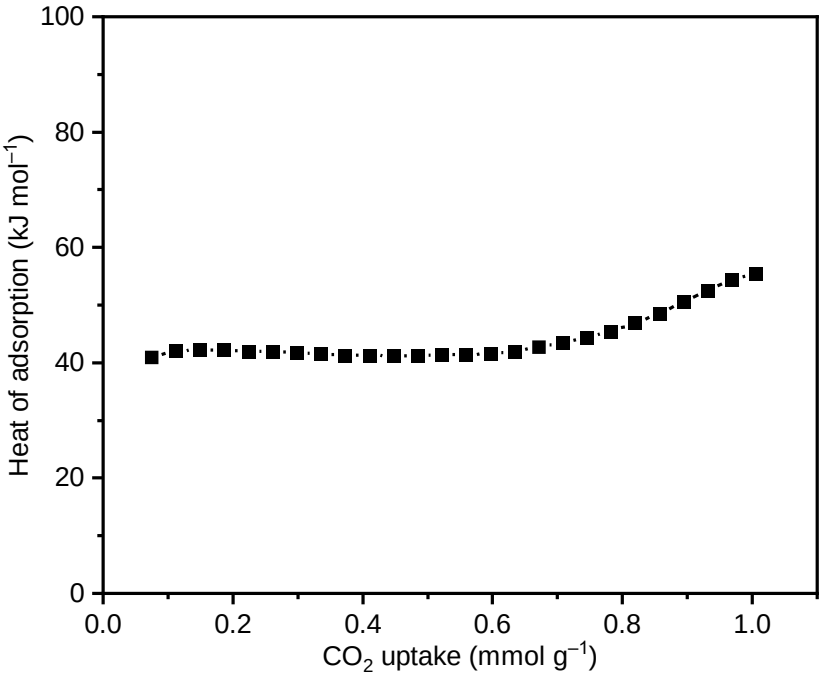

Supplementary Fig. 6 | Estimated isosteric heat of CO_2 adsorption of COF-999 plotted as a function of uptake determined through the Clausius-Clapeyron equation using CO_2 sorption isotherms at 15 °C to 35 °C. The CO_2 isotherm at 35 °C showed a turning point from a steep increase to a moderate slope at around 1 mmol g^{-1}, indicating the transformation from chemisorption to physisorption. However, the isotherm at 15 °C and 25 °C maintained chemisorption at this point, making the Clausius-Clapeyron equation not applicable when uptake is higher than 1 mmol g^{-1}.

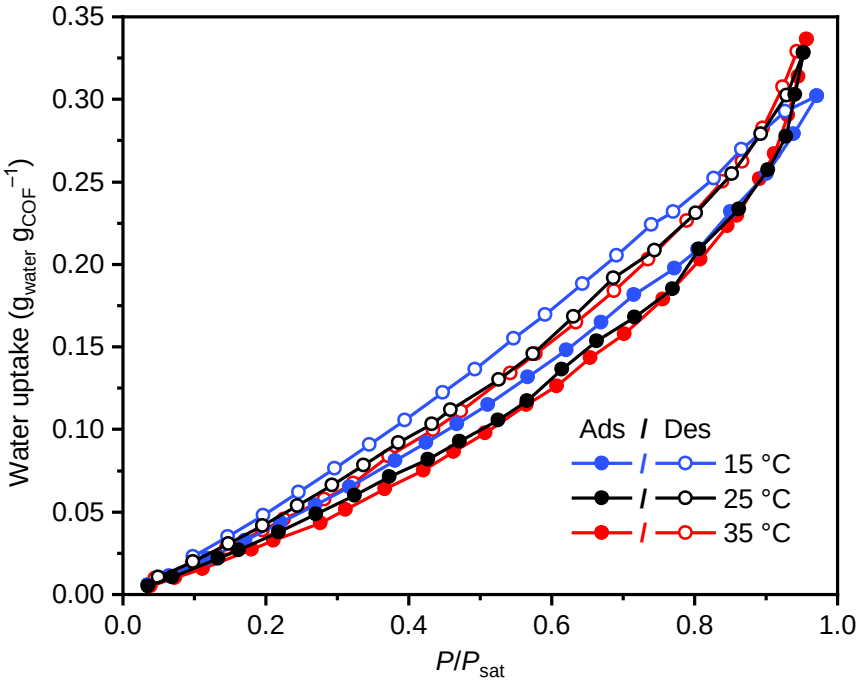

Supplementary Fig. 7 | Single-component water vapor sorption isotherms of COF-999 measured at 15 °C (blue), 25 °C (black), and 35 °C (red). *P*, water vapor pressure; P_{sat}, saturation water vapor pressure at the analysis temperature.

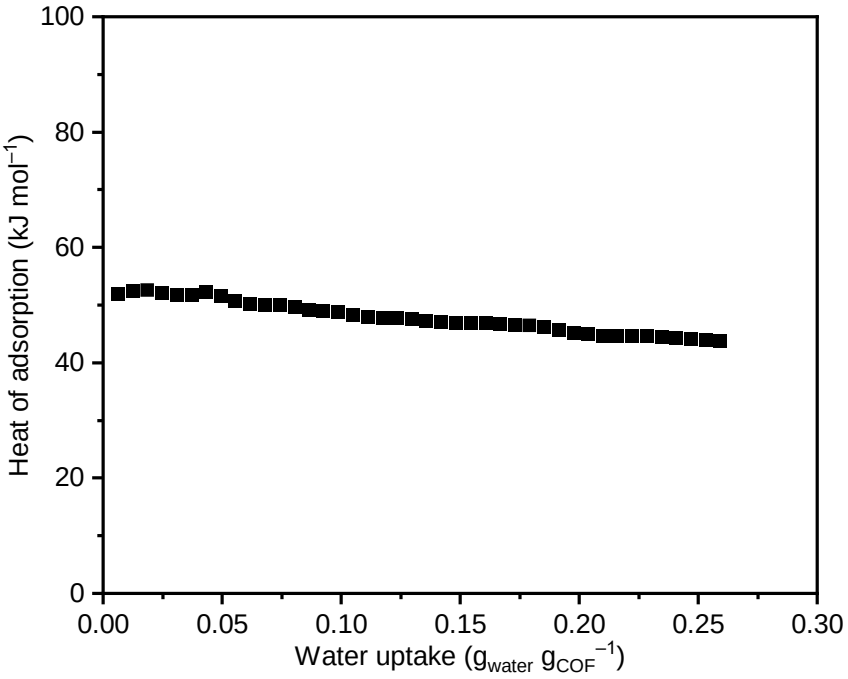

Supplementary Fig. 8 | Estimated isosteric heat of water vapor adsorption of COF-999 plotted as a function of uptake determined through the Clausius-Clapeyron equation using water vapor sorption isotherms at 15 °C to 35 °C.

Section 6. Fourier-Transform Infrared Spectroscopy (FT-IR)

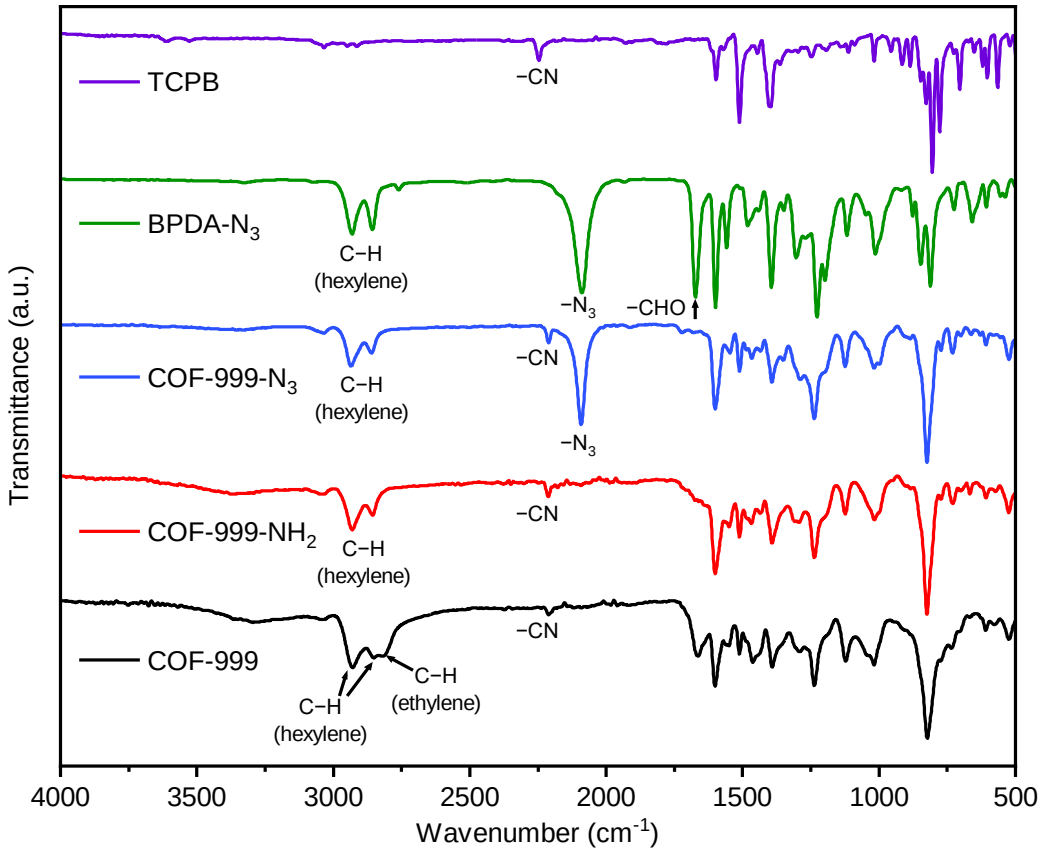

Supplementary Fig. 9 | Stacked FT-IR spectra of TCPB (violet), BPDA-N_3 (green), COF-999-N_3 (blue), COF-999-NH_2 (red), and COF-999 (black). The transmittance values along the Y−axis were normalized for comparison. As shown in the figure, the disappearance of the azide vibration at 2089 cm^{-1} (azide $\nu_{N=N}$ stretch) in COF-999-NH_2 indicated the completion of Staudinger reduction. The emergence of C−H vibration at 2819 cm^{-1} (ethylene ν_{C-H} stretch) in COF-999 indicated the successful loading of polyamine.

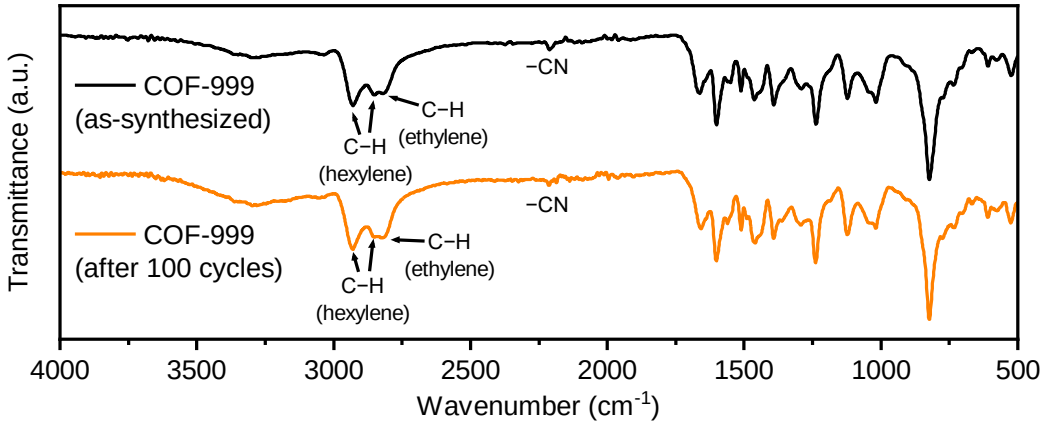

Supplementary Fig. 10 | Comparison of FT-IR spectra of as-synthesized COF-999 (black) and sample after 100 outdoor air cycles (orange).

Section 7. Powder X-ray Diffraction (PXRD)

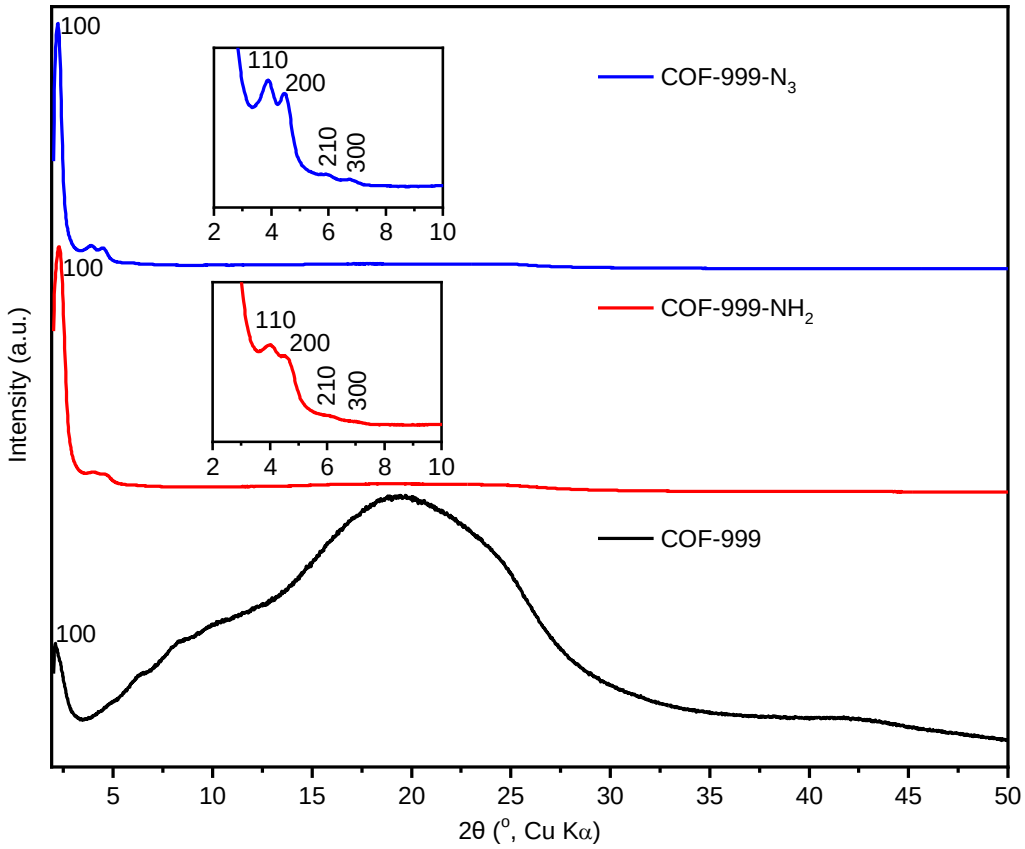

Supplementary Fig. 11 | PXRD spectra of COF-999-N_3 (blue), COF-999-NH_2 (red), and COF-999 (black). The intensity values along the Y−axis were normalized for comparison. The disordered polyamines inside the pores lead to weakened diffraction peaks of COF-999.

Supplementary Table 3 | Fractional atomic coordinates of the structural model of COF-999-N_3, resulting from Pawley refinement.

COF-999-N_3			
Hexagonal, *P*6 $a = b = 45.524(2)$ Å, $c = 3.94(9)$ Å $\alpha = \beta = 90°$, $\gamma = 120°$ $R_p = 1.81\%$, $R_{wp} = 3.12\%$			
Atom	***x***	***y***	***z***
C1	0.01805	-0.49136	-0.25158
C2	0.03581	-0.50821	-0.16051
C3	0.07179	-0.49107	-0.15523
C4	0.09034	-0.45676	-0.25528
C5	0.07261	-0.44028	-0.35545
C6	0.03718	-0.45696	-0.34496
C7	0.12822	-0.43965	-0.27656
C8	0.1504	-0.4071	-0.19325
C9	0.18767	-0.39329	-0.22082
C10	0.13919	-0.3849	-0.05727
N11	0.13036	-0.367	0.052
C12	0.20318	-0.41021	-0.07373
C13	0.23856	-0.39575	-0.0798
C14	0.25942	-0.36426	-0.23963
C15	0.24352	-0.3479	-0.39378
C16	0.20826	-0.36197	-0.38005
C17	0.29743	-0.34838	-0.24197
C18	0.31855	-0.3128	-0.24193
O19	0.09044	-0.50657	-0.04816
C20	0.07259	-0.54088	0.06726
C21	0.09827	-0.55133	0.17538
C22	0.0808	-0.58922	0.26091
C23	0.10672	-0.59965	0.36627
C24	0.0893	-0.63764	0.44742
C25	0.11502	-0.648	0.55845
N26	0.09736	-0.68328	0.6576
H27	0.02141	-0.53431	-0.07921
H28	0.086	-0.41464	-0.45186
H29	0.02481	-0.44326	-0.43061
H30	0.13856	-0.45533	-0.35981
H31	0.18799	-0.43403	0.0576
H32	0.24949	-0.40889	0.051
H33	0.25818	-0.3243	-0.52957
H34	0.19695	-0.34851	-0.49803
H35	0.30715	-0.29692	-0.24098
H36	0.05652	-0.55778	-0.13954
H37	0.05638	-0.54321	0.28736
H38	0.11248	-0.53597	0.39836
H39	0.11684	-0.54557	-0.03148
H40	0.06648	-0.60433	0.03746

H41	0.06227	-0.59495	0.46814
H42	0.12083	-0.58475	0.59143
H43	0.12544	-0.59362	0.16031
H44	0.07553	-0.65268	0.22122
H45	0.07034	-0.64372	0.6513
H46	0.13012	-0.63191	0.77439
H47	0.13266	-0.64408	0.34628
N48	0.69279	0.80941	0.75625
N49	0.70231	0.83812	0.85499

Supplementary Table 4 | Fractional atomic coordinates of the structural model of COF-999-NH_2, resulting from Pawley refinement.

COF-999-NH_2			
Hexagonal, *P*6 $a = b = 44.795(6)$ Å, $c = 3.945(2)$ Å $\alpha = \beta = 90°$, $\gamma = 120°$ $R_p = 1.55\%$, $R_{wp} = 2.21\%$			
Atom	***x***	***y***	***z***
C1	0.01817	-0.4907	-0.30415
C2	0.03711	-0.50661	-0.20596
C3	0.07349	-0.48792	-0.19657
C4	0.09093	-0.45317	-0.29938
C5	0.07205	-0.43767	-0.40795
C6	0.0362	-0.45587	-0.40206
C7	0.12908	-0.43437	-0.31041
C8	0.14988	-0.40153	-0.21241
C9	0.18749	-0.38726	-0.21407
C10	0.1369	-0.37996	-0.08499
N11	0.12668	-0.36252	0.01702
C12	0.20191	-0.40506	-0.05408
C13	0.23747	-0.39164	-0.05501
C14	0.25941	-0.36046	-0.22288
C15	0.24472	-0.34276	-0.38356
C16	0.20916	-0.35581	-0.37494
C17	0.29735	-0.34653	-0.22885
C18	0.32028	-0.31082	-0.22964
O19	0.0936	-0.50214	-0.08155
C20	0.0767	-0.53713	0.03037
C21	0.10389	-0.54608	0.14367
C22	0.08769	-0.58461	0.22314
C23	0.11513	-0.59352	0.33368
C24	0.09906	-0.63221	0.40384
C25	0.12648	-0.6411	0.51743
N26	0.11136	-0.67798	0.58267
H27	0.02328	-0.53309	-0.12163
H28	0.0849	-0.41163	-0.50499
H29	0.02266	-0.44306	-0.4927
H30	0.14092	-0.44923	-0.39034
H31	0.18564	-0.42902	0.07828
H32	0.24769	-0.40544	0.08277
H33	0.26048	-0.31924	-0.52368
H34	0.19842	-0.3419	-0.50266
H35	0.31017	-0.29341	-0.22905
H36	0.06134	-0.55449	-0.17985
H37	0.05946	-0.54062	0.24726
H38	0.11726	-0.53051	0.37074
H39	0.12347	-0.53892	-0.0589
H40	0.07425	-0.59991	-0.00476

H41	0.06812	-0.59177	0.42585
H42	0.12818	-0.57871	0.56495
H43	0.13502	-0.58579	0.13331
H44	0.08622	-0.64703	0.17187
H45	0.07902	-0.64	0.60279
H46	0.13928	-0.6266	0.75081
H47	0.14674	-0.63326	0.32055
H48	0.10084	-0.6914	0.35707
H49	0.09114	-0.68575	0.75574

Supplementary Table 5 | Fractional atomic coordinates of the structural model of COF-999, resulting from geometric optimization.

COF-999							
Monoclinic, *P*2 *a* = 45.3710 Å, *b*= 4.2871 Å, *c* = 43.7961 Å $\alpha = \gamma = 90°$, $\beta = 61.6179°$							
Atom	***x***	***y***	***z***	**Atom**	***x***	***y***	***z***
C1	-0.51187	-0.20455	-0.00702	H9	0.70096	-0.41878	-0.89971
C2	-0.98173	-0.21315	-0.01095	H13	-0.05266	-0.333	-0.8858
C3	-0.50818	-0.18003	-0.48088	H14	0.44536	-0.24728	-0.56074
C7	0.45712	-0.35551	-0.98893	H15	-0.38909	-0.3722	-0.06294
C8	0.03271	-0.36282	-0.04328	H19	-0.04548	-0.74402	-0.89715
C9	-0.49179	-0.3076	-0.46354	H20	0.44865	-0.66083	-0.55353
C13	-0.56463	-0.38203	-0.00358	H21	-0.40406	-0.77331	-0.05513
C14	-0.93215	-0.38075	-0.06367	H25	-0.09779	-0.88735	-0.84611
C15	-0.50807	-0.32992	-0.42689	H26	0.45137	-0.78946	-0.60959
C19	-0.55456	-0.25471	-0.03678	H27	-0.35392	-0.938	-0.05101
C20	-0.91173	-0.25013	-0.05078	H31	-0.11038	-0.48459	-0.83693
C21	-0.54179	-0.23117	-0.40809	H32	0.45204	-0.38086	-0.62001
C25	-0.52441	-0.08662	-0.05356	H33	-0.3401	-0.539	-0.05459
C26	-0.92657	-0.0824	-0.0194	H37	-0.06105	-0.37628	-0.82726
C27	-0.55685	-0.08073	-0.4257	H38	0.39577	-0.30722	-0.5682
C31	-0.50299	-0.06619	-0.03911	H39	-0.33581	-0.50504	-0.11399
C32	0.03876	-0.06983	-0.99934	H43	-0.049	-0.78096	-0.83534
C33	0.45953	-0.05956	-0.46168	H44	0.39497	-0.71248	-0.55696
C37	-0.57674	-0.28618	-0.05292	H45	-0.34819	-0.90883	-0.11076
C38	-0.87478	-0.27506	-0.07144	H49	-0.10271	-0.93851	-0.78432
C39	-0.5604	-0.26851	-0.36978	H50	0.39607	-0.86644	-0.61281
C43	-0.56611	-0.36085	-0.08653	H51	-0.29795	-1.07081	-0.10597
C44	-0.85392	-0.33338	-0.05814	H55	-0.11674	-0.53819	-0.77709
C45	-0.59333	-0.34086	-0.35129	H56	0.3969	-0.46	-0.62409
C49	-0.59002	-0.38561	-0.1009	H57	-0.28608	-0.66868	-0.10615
C50	-0.81706	-0.35527	-0.08107	H61	-0.06767	-0.39368	-0.76803
C51	-0.61045	-0.35191	-0.3126	H62	0.3423	-0.36958	-0.57139
C55	-0.53116	-0.43393	-0.1092	H63	-0.28004	-0.59857	-0.16566
C56	-0.86699	-0.39797	-0.02141	H67	-0.05437	-0.79513	-0.77443
C57	-0.61262	-0.42523	-0.36864	H68	0.34167	-0.76525	-0.55747
C61	-0.62005	-0.21324	-0.08686	H69	-0.29212	-0.99949	-0.16554
C62	-0.80085	-0.18297	-0.11215	H73	-0.10809	-0.95002	-0.72282
C63	-0.59897	-0.17233	-0.29348	H74	0.33914	-0.95926	-0.61012
C67	-0.64142	-0.22952	-0.10155	H75	-0.24228	-1.17734	-0.15996
C68	-0.76618	-0.20275	-0.13304	H79	-0.1221	-0.54896	-0.71711
C69	-0.61508	-0.18518	-0.25735	H80	0.33988	-0.56058	-0.62404
C73	-0.63312	-0.4157	-0.1309	H81	-0.23074	-0.77679	-0.15868
C74	-0.74682	-0.39226	-0.12328	H85	-0.20015	-0.98392	-0.2148
C75	-0.64339	-0.37474	-0.23927	H87	-0.06203	-0.79725	-0.71477
C79	-0.60348	-0.59056	-0.14473	H88	0.28907	-0.84245	-0.55758
C80	-0.76294	-0.56464	-0.0924	H89	-0.23459	-1.10317	-0.21628

C81	-0.65566	-0.54643	-0.25804	H93	0.75442	-0.06037	-0.84378
C85	-0.5822	-0.57598	-0.12999	H94	0.60581	-0.04134	-0.75655
C86	-0.79753	-0.54543	-0.07156	H95	0.66372	-0.08594	-0.90915
C87	-0.6394	-0.53589	-0.29424	H99	0.74889	-0.7187	-0.91546
C91	-0.65453	-0.41619	-0.148	H100	0.67727	-0.69686	-0.75521
C92	-0.70983	-0.40317	-0.14453	H101	0.59681	-0.74163	-0.83312
C93	-0.65959	-0.39446	-0.20096	H105	0.80899	-0.68445	-0.95187
C97	-0.63983	-0.40735	-0.18428	H106	0.64919	-0.67746	-0.69219
C98	-0.68954	-0.41453	-0.12833	H107	0.55968	-0.71607	-0.85862
C99	-0.69462	-0.3948	-0.18094	H111	0.86456	-0.26442	-0.90063
C103	0.38959	-0.59389	-0.95048	H112	0.54568	-0.24674	-0.64359
C104	0.06487	-0.55961	-0.11482	H113	0.60332	-0.26437	-0.96449
C105	-0.45631	-0.47398	-0.42653	H117	-0.08867	0.03964	0.01037
C109	0.3536	-0.7076	-0.93719	H118	-0.41851	0.02153	-0.58835
C110	0.08853	-0.64535	-0.15267	H119	0.51725	0.0282	-0.92195
C111	-0.44259	-0.55342	-0.40152	H123	-0.0279	0.05286	-0.02523
C115	0.33521	-0.73465	-0.8975	H124	-0.44697	0.05029	-0.5254
C116	0.07069	-0.61811	-0.17483	H125	0.47945	0.05732	-0.94704
C117	-0.40412	-0.5451	-0.421	H129	-0.01633	-0.47259	-0.94833
C121	0.29864	-0.8337	-0.88411	H130	0.46668	-0.39638	-0.52094
C122	0.09433	-0.69181	-0.21317	H131	-0.45082	-0.46075	-0.03585
C123	-0.38829	-0.62761	-0.39788	H135	0.09993	0.07898	-0.42856
C127	0.27961	-0.836	-0.84433	H136	-0.17448	-0.05904	-0.4179
C128	0.07656	-0.63896	-0.23505	H139	0.06847	-0.01944	-0.38557
C129	-0.34995	-0.61238	-0.41938	H140	-0.19155	-0.19814	-0.44417
C133	0.24316	-0.93696	-0.83097	H143	0.04436	-0.4734	-0.37922
C134	0.09974	-0.70254	-0.27366	H144	-0.14564	-0.93882	-0.48515
C135	-0.33204	-0.71494	-0.39895	H147	0.07361	-0.41331	-0.42429
C139	0.08344	-0.82625	-0.40225	H148	-0.17652	-0.64607	-0.47499
C140	-0.18707	-0.98506	-0.43314	H151	0.04555	-0.95689	-0.42713
C143	0.059	-0.59074	-0.40463	H153	0.12565	-0.39994	-0.43222
C144	-0.16303	-0.78189	-0.46399	H154	-0.19579	-0.54082	-0.39054
C147	0.12974	-0.47214	-0.41017	H157	0.12935	-0.25905	-0.39565
C148	-0.22081	-0.64365	-0.38258	H158	-0.23876	-0.44827	-0.37678
C151	0.16476	-0.61319	-0.42524	H161	0.17193	-0.62394	-0.40422
C152	-0.23158	-0.83504	-0.34957	H162	-0.25726	-0.92739	-0.34112
C155	0.0022	-0.76803	-0.38824	H165	0.1644	0.14527	-0.43416
C157	-0.02022	-0.88188	-0.40333	H166	-0.2148	-0.0405	-0.35589
C159	0.22182	-0.42373	-0.45743	H169	0.1899	-0.52178	-0.47744
C160	-0.26265	-0.58231	-0.29362	H170	-0.21584	-0.77929	-0.31306
C163	0.24764	-0.28546	-0.49216	H173	-0.00728	-0.53789	-0.37568
C164	-0.25996	-0.44184	-0.26296	H175	0.00115	-0.93521	-0.36831
C167	0.10375	-0.68592	-0.33072	H177	-0.0171	-0.72598	-0.42492
C168	-0.27726	-0.79006	-0.40324	H179	-0.01249	-1.12017	-0.41402
C171	0.08472	-0.60569	-0.35072	H181	-0.05845	-1.02768	-0.35651
C172	-0.23962	-0.74008	-0.42691	H183	-0.06301	-0.66081	-0.36775
N1	-0.50328	-0.49202	-0.1273	H185	0.22957	-0.66445	-0.45502
N2	0.12271	-0.44949	-0.99222	H186	-0.27788	-0.79935	-0.28454
N3	0.37192	-0.49216	-0.38233	H189	0.22119	-0.27955	-0.43601

N7	0.22516	-0.92675	-0.79312	H190	-0.27569	-0.41462	-0.30249
N8	0.08184	-0.63766	-0.29342	H193	0.23887	-0.0541	-0.49597
N9	-0.2957	-0.69102	-0.42143	H194	-0.24392	-0.23021	-0.27165
N13	0.03672	-0.73694	-0.41635	H197	0.2505	-0.43961	-0.51381
N15	0.18836	-0.42399	-0.4548	H198	-0.24822	-0.61323	-0.25292
N16	-0.22926	-0.64884	-0.32257	H201	0.28989	-0.47269	-0.49402
N19	-0.05554	-0.88676	-0.37723	H202	-0.30602	-0.56506	-0.22393
N21	0.27981	-0.2505	-0.49256	H205	0.29609	-0.13501	-0.51542
N22	-0.29325	-0.35888	-0.23547	H206	-0.29032	-0.23824	-0.21638
N25	0.10434	-0.70062	-0.38748	H209	0.12621	-0.53326	-0.34006
N26	-0.22025	-0.84891	-0.40983	H210	-0.2856	-0.65105	-0.3791
N29	-0.14324	-0.57591	-0.45429	H213	0.11213	-0.9335	-0.3358
O1	0.40441	-0.54084	-0.98704	H214	-0.28205	-1.0411	-0.39613
O2	0.08354	-0.53168	-0.09628	H217	0.06039	-0.73306	-0.33805
O3	-0.4921	-0.44969	-0.40833	H218	-0.23224	-0.87434	-0.45122
H1	0.81464	-0.02431	-0.88014	H221	0.0787	-0.3528	-0.34827
H2	0.57801	-0.01426	-0.69383	H222	-0.23487	-0.49015	-0.43389
H3	0.62662	-0.05456	-0.93461	H225	-0.12791	-0.71234	-0.44782
H7	0.70998	-0.38505	-0.80627	H226	-0.12714	-0.4499	-0.47644
H8	0.61279	-0.40656	-0.80035				

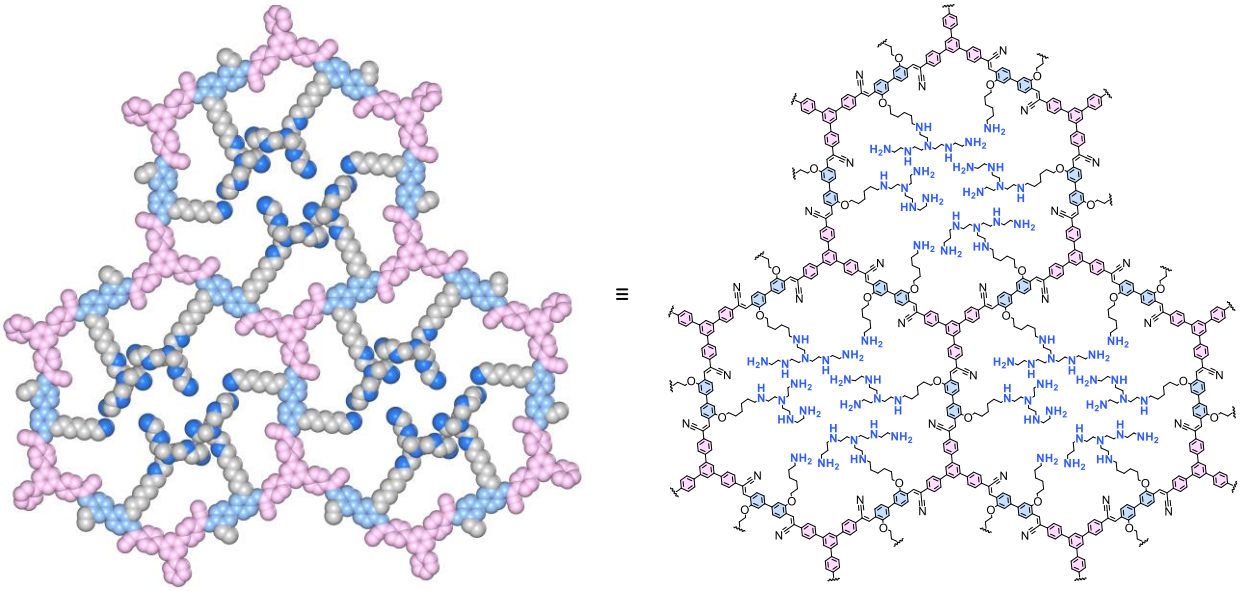

Space filling model of COF-999

Chemical structure of COF-999

Section 8. Thermogravimetric Analyses (TGA)

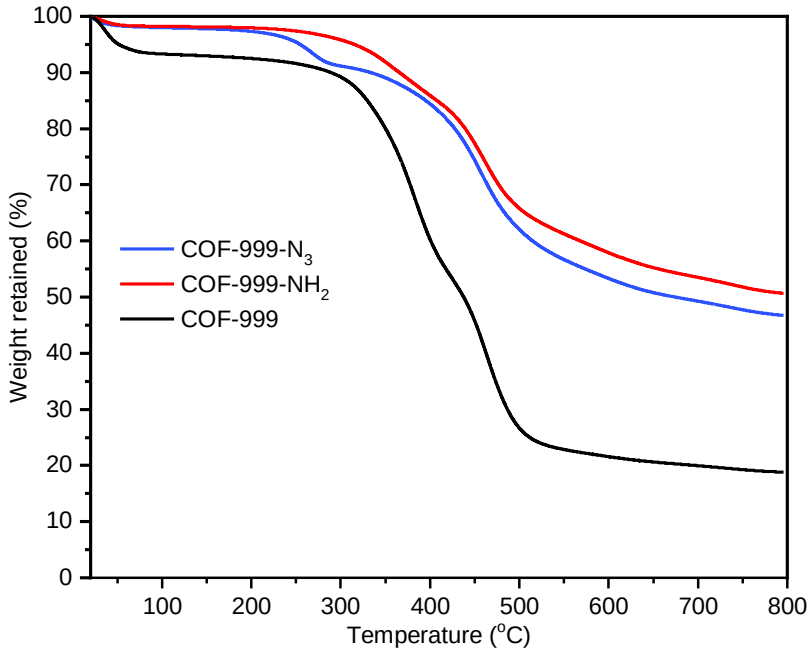

Supplementary Fig. 12 | TGA curves COF-999-N_3 (blue), COF-999-NH_2 (red), and COF-999 (black). Measurements were conducted under a continuous flow of N_2.

COF-999-N_3 exhibited 3 major steps of weight loss, including desorption of adsorbed molecules (25–50 °C, 1.4 wt. %), decomposition of azides (200–315 °C, 7.9 wt.), and decomposition of the framework (315–800 °C, 43.9 wt. %).

COF-999-NH_2 exhibited 2 major steps of weight loss, including desorption of adsorbed molecules (25–50 °C, 1.4 wt. %) and decomposition of the framework (250–800 °C, 48.0 wt. %).

COF-999 exhibited 2 major steps of weight loss, including desorption of adsorbed molecules (25–65 °C, 6.0 wt. %) and decomposition of the framework (250–800 °C, 75.2 wt. %).

In COF-999, a larger initial weight loss was observed from 25 to 65 °C, which can be attributed to the higher CO_2 capacity. The temperature of weight loss also matches the desorption temperature of CO_2.

The backbone of all three COFs began to decompose at 250 °C, however, the decomposition process of COF-999 occurred more rapidly. This rapid decomposition can be attributed to the steric repulsion of the added polyamine groups, which weakens the interlayer interactions and forces the layers apart under high temperatures[30].

At 800 °C, COF-999 also exhibited greater weight loss compared to the other two COFs. This can be attributed to two factors: (i) The polyethyleneimine chain in COF-999 would be completely decomposed under high temperature hence resulting in more weight loss[31], and (ii) the basicity of the polyamine could influence the thermostability of the COF backbone, leading to more complete decomposition of COF backbone when exposed to high temperatures. This has also been observed in other amine-functionalized COFs[1].

Section 9. Calculation of Degree of Polymerization

The area of the peak in multiCP/MAS ssNMR spectrum (Supplementary Fig. 13) is proportional to the number of atoms that it represents[32]. Since there are 6 carbons (C-#1 to C-#6) on the side chain before the polymerization reaction, and each polyethylenimine unit provides two additional carbons on the side chain, the average degree of polymerization can be calculated as (12.10 – 6) / 2 = 3.05 per side chain. This number can also be calculated from the elemental analysis results of COF-999 (Supplementary Table 6)

From multiCP/MAS ^{15}N ssNMR spectrum (Supplementary Fig. 14), 65.9% of the amines on the pore wall were linked with polyethylenimine units, so the degree of polymerization after excluding those non-reacted amines can be calculated as 3.05 / (65.9%) = 4.63.

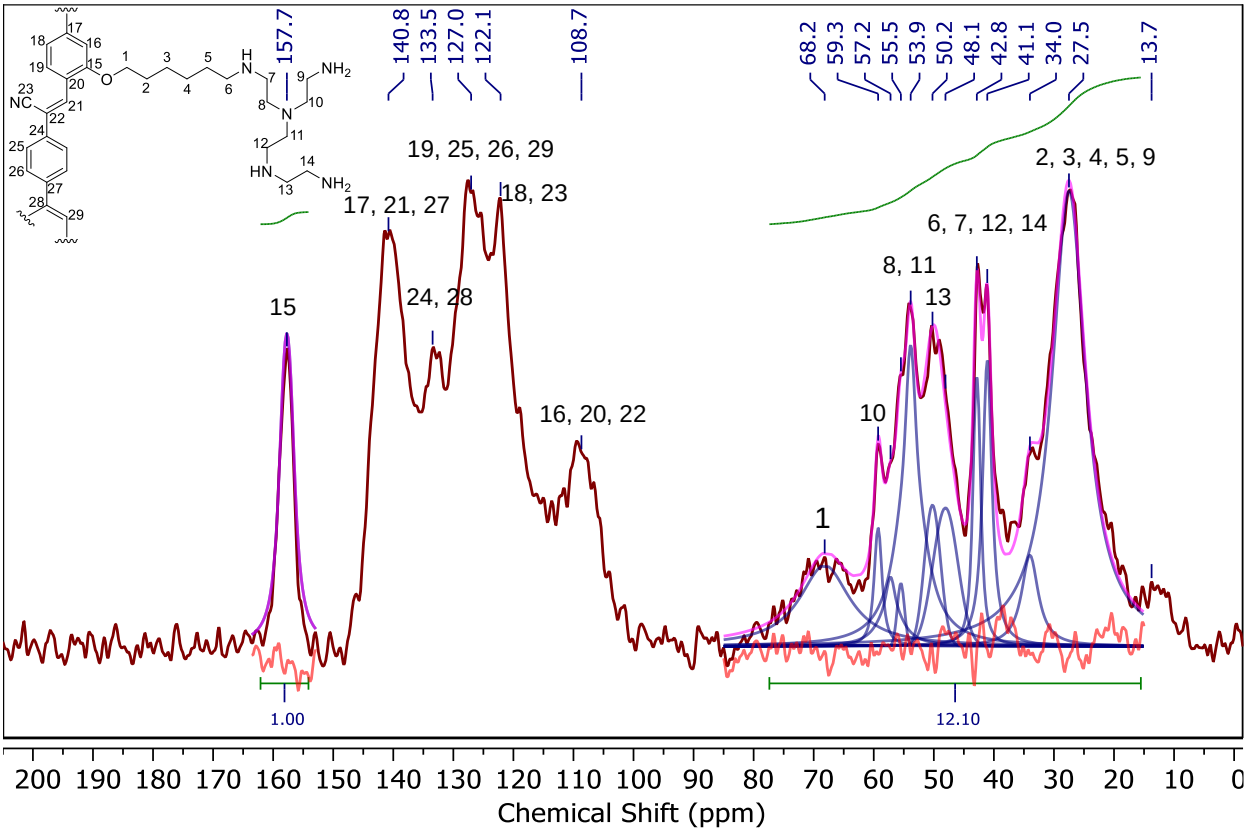

Supplementary Fig. 13 | Linear deconvolution of quantitative multiCP/MAS ^{13}C ssNMR spectrum of COF-999. The peak at 157.7 ppm can be assigned to C-#15, and the region from 80 to 13 ppm can be assigned to carbons on the side chain (C-#1 to C-#14). The ratio of the integrated area of those two regions was 1.00:12.10. Color code for lines: experimental data, brown; simulated peak profiles, blue; sum of simulated signals, violet; simulation-experiment difference, red.

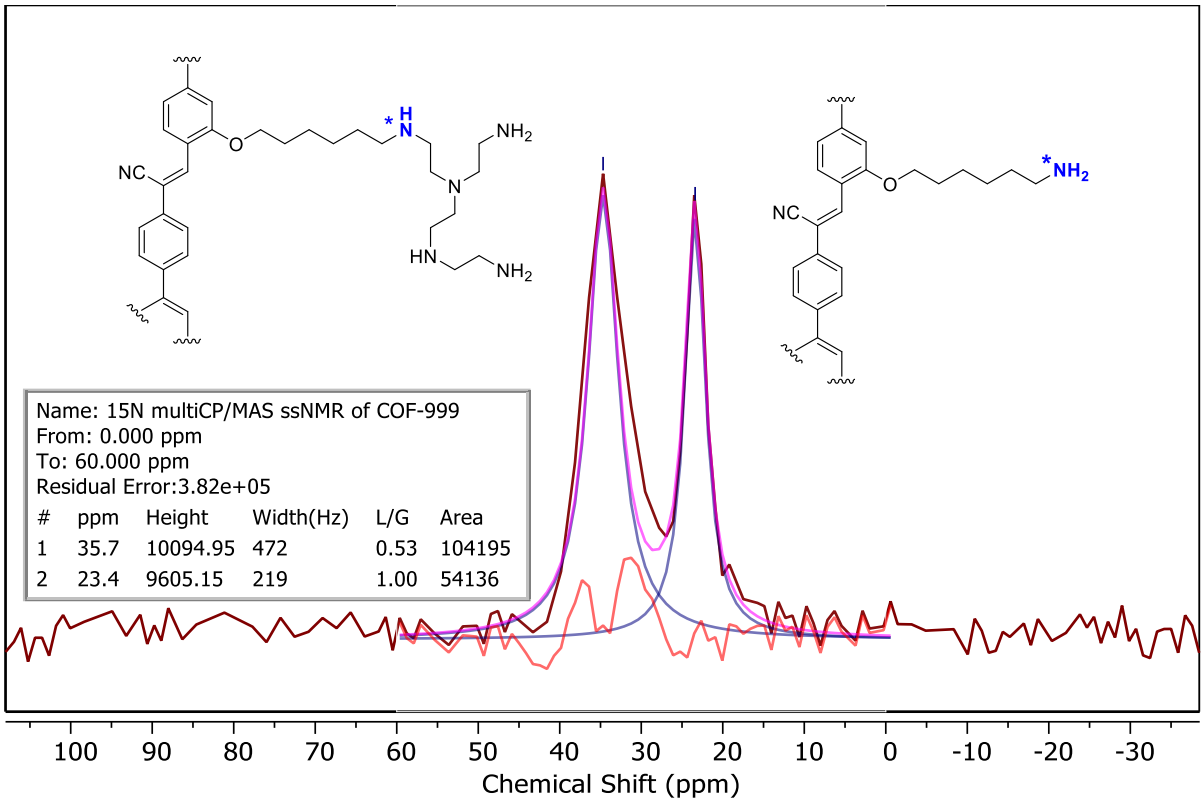

Supplementary Fig. 14 | Linear deconvolution of quantitative multiCP/MAS ^{15}N ssNMR spectrum of ^{15}N labeled COF-999. The peak at 35.7 ppm can be assigned to the amines reacted with aziridine, and the peak at 23.4 ppm can be assigned to unreacted amines. Signals from unlabeled nitrogen (aziridine and nitrile) can be neglected due to their low natural abundance. The ratio of the integrated area of those two peaks was 0.659:0.341. Color code for lines: experimental data, brown; simulated peak profiles, blue; sum of simulated signals, violet; simulation-experiment difference, red.

Supplementary Table 6 | Comparison of the experimental elemental analysis result of COF-999 [$C_{23}H_{23}N_2O\cdot(C_2H_5N)_n$] with calculated elements ratio of different degrees of polymerization. The experimental C/N ratio matches with the calculated result of n=3.1.

Degree of polymerization	C (%)	N (%)	H (%)	C/N mass ratio
n = 2.5	74.55	13.97	7.93	5.34
n = 2.6	74.37	14.15	7.97	5.26
n = 2.7	74.20	14.32	8.00	5.18
n = 2.8	74.03	14.49	8.04	5.11
n = 2.9	73.86	14.66	8.07	5.04
n = 3.0	73.69	14.82	8.10	4.97
n = 3.1	73.53	14.98	8.14	4.91
n = 3.2	73.37	15.14	8.17	4.85
n = 3.3	73.22	15.29	8.20	4.79
n = 3.4	73.06	15.44	8.23	4.73
n = 3.5	72.91	15.59	8.26	4.68
Experimental data from elemental analysis	70.19	14.35	7.24	4.89

Section 10. Dynamic Breakthrough Measurements

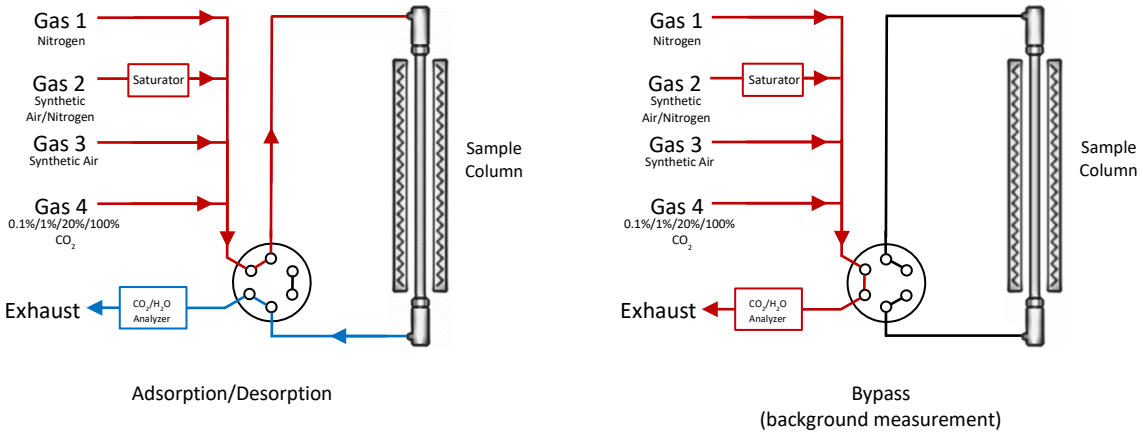

Supplementary Fig. 15 | Schematic diagram of the breakthrough instrument. The adsorption/desorption mode and bypass mode were controlled by a 6-port valve.

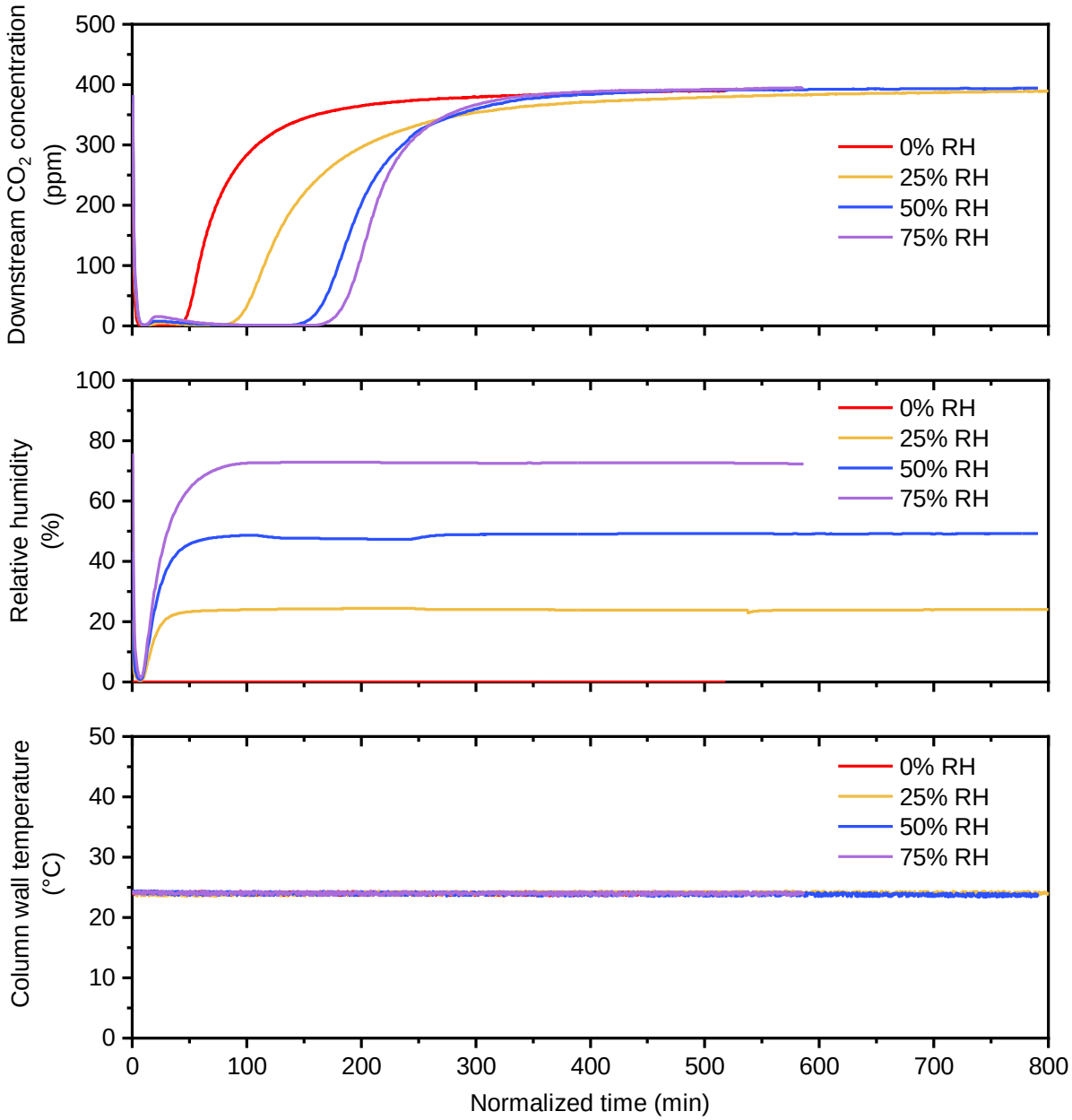

Supplementary Fig. 16 | Dynamic breakthrough measurements of COF-999 at 400 ppm of CO_2 with 0% (red), 25% (yellow), 50% (blue), and 75% (purple) RH at 25°C. The breakthrough time was normalized to 100 mg of COF-999 sample for comparison. The CO_2 uptakes shown in this figure were calculated to be 0.95, 1.76, 2.02, and 2.06 mmol g^{-1}, respectively. This experiment was reproduced three times using different batches of samples (see Supplementary Fig. 17).

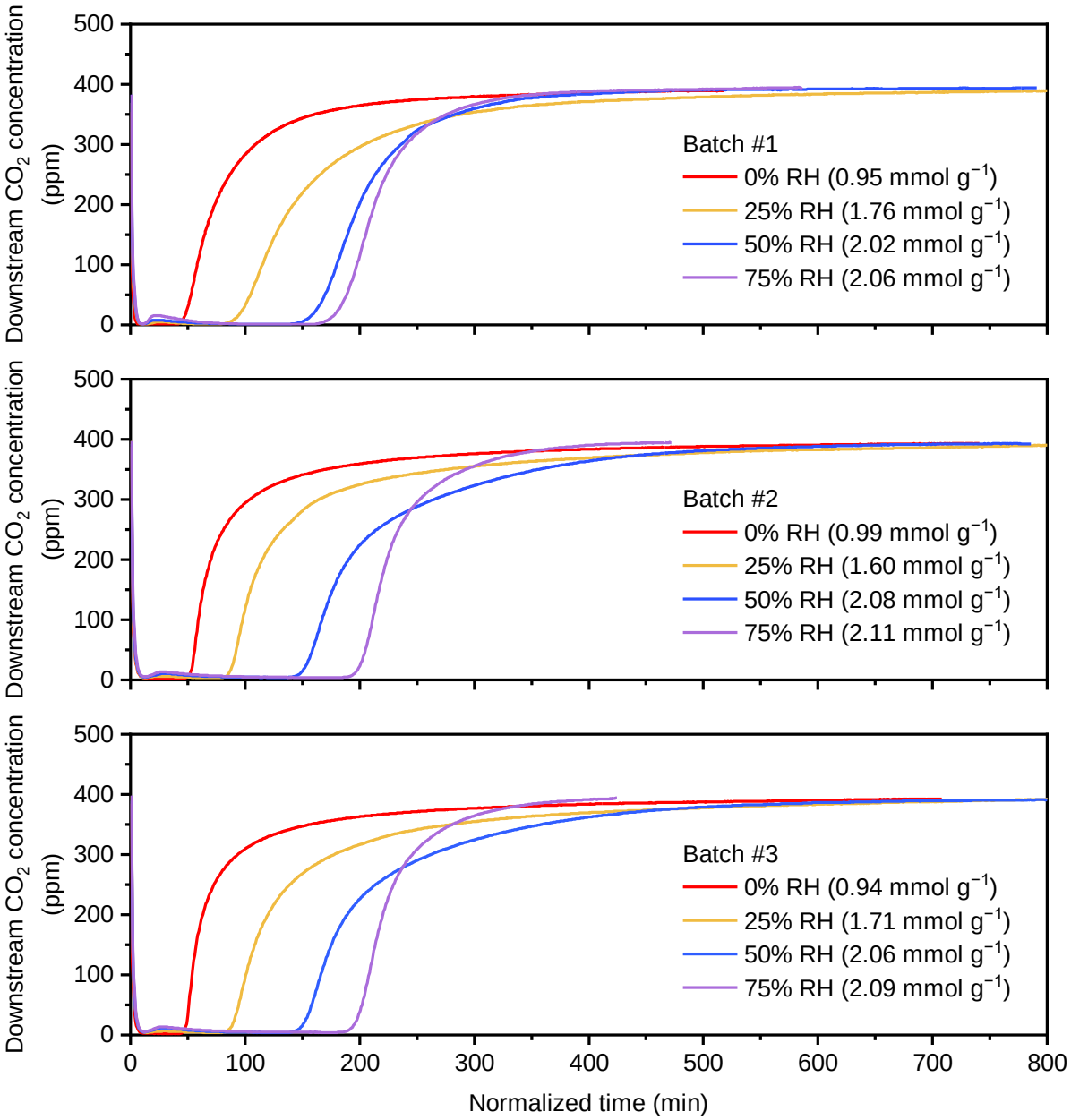

Supplementary Fig. 17 | CO_2 breakthrough curves of COF-999 at 400 ppm of CO_2 with 0% (red), 25% (yellow), 50% (blue), and 75% (purple) RH at 25°C. Three different batches of samples were synthesized for the measurement. The breakthrough time was normalized to 100 mg of COF-999 sample for comparison. The breakthrough curves for batch #1 are the same as shown in Supplementary Fig. 16.

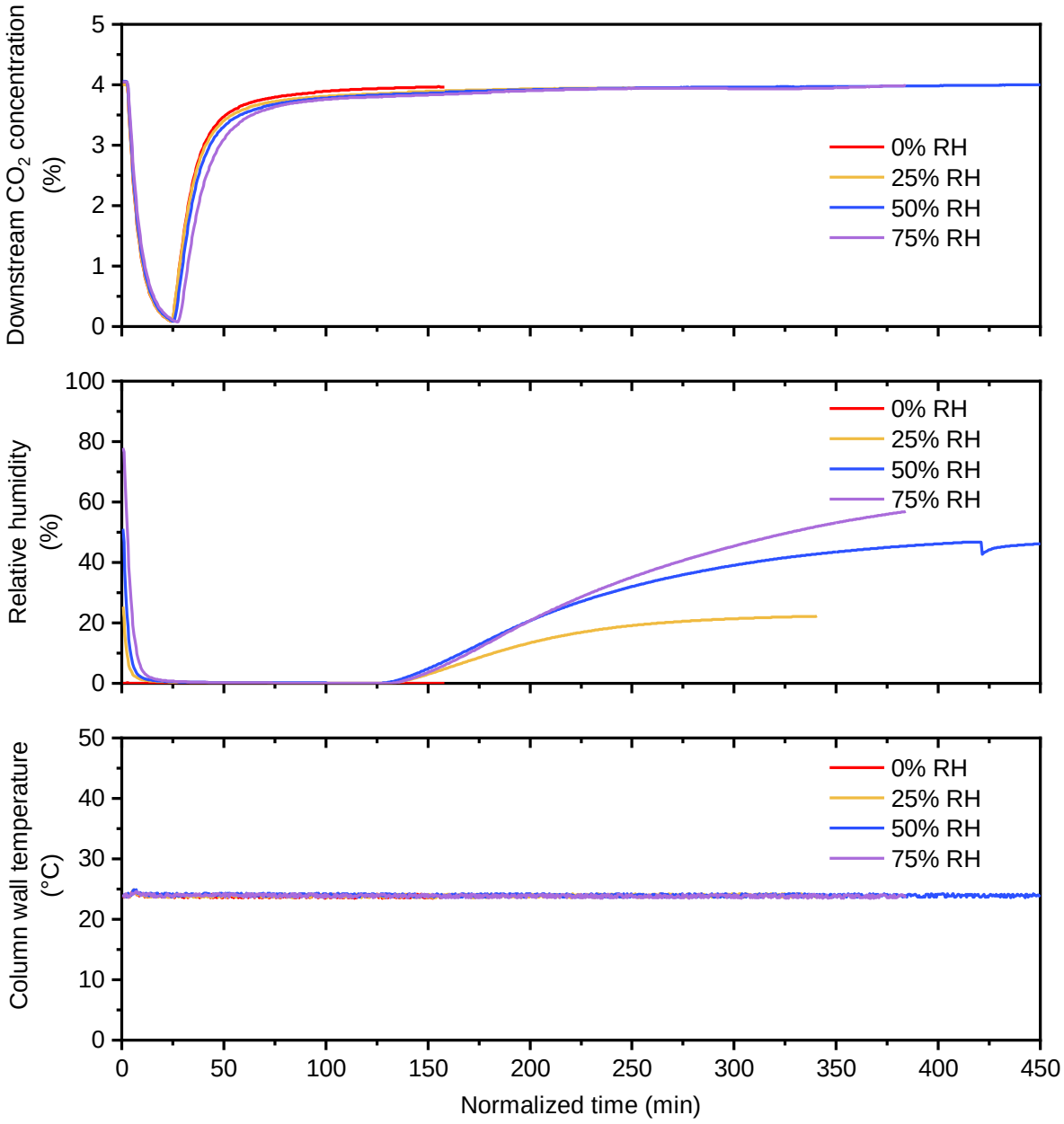

Supplementary Fig. 18 | Dynamic breakthrough measurements of COF-999 at 4% of CO_2 with 0% (red), 25% (yellow), 50% (blue), and 75% (purple) RH at 25°C. 280 mg COF-999 sample and 0.96 cm s^{-1} gas velocity were used in the measurement. The CO_2 uptakes were calculated to be 2.09, 2.39, 3.03, and 3.17 mmol g^{-1}, respectively.

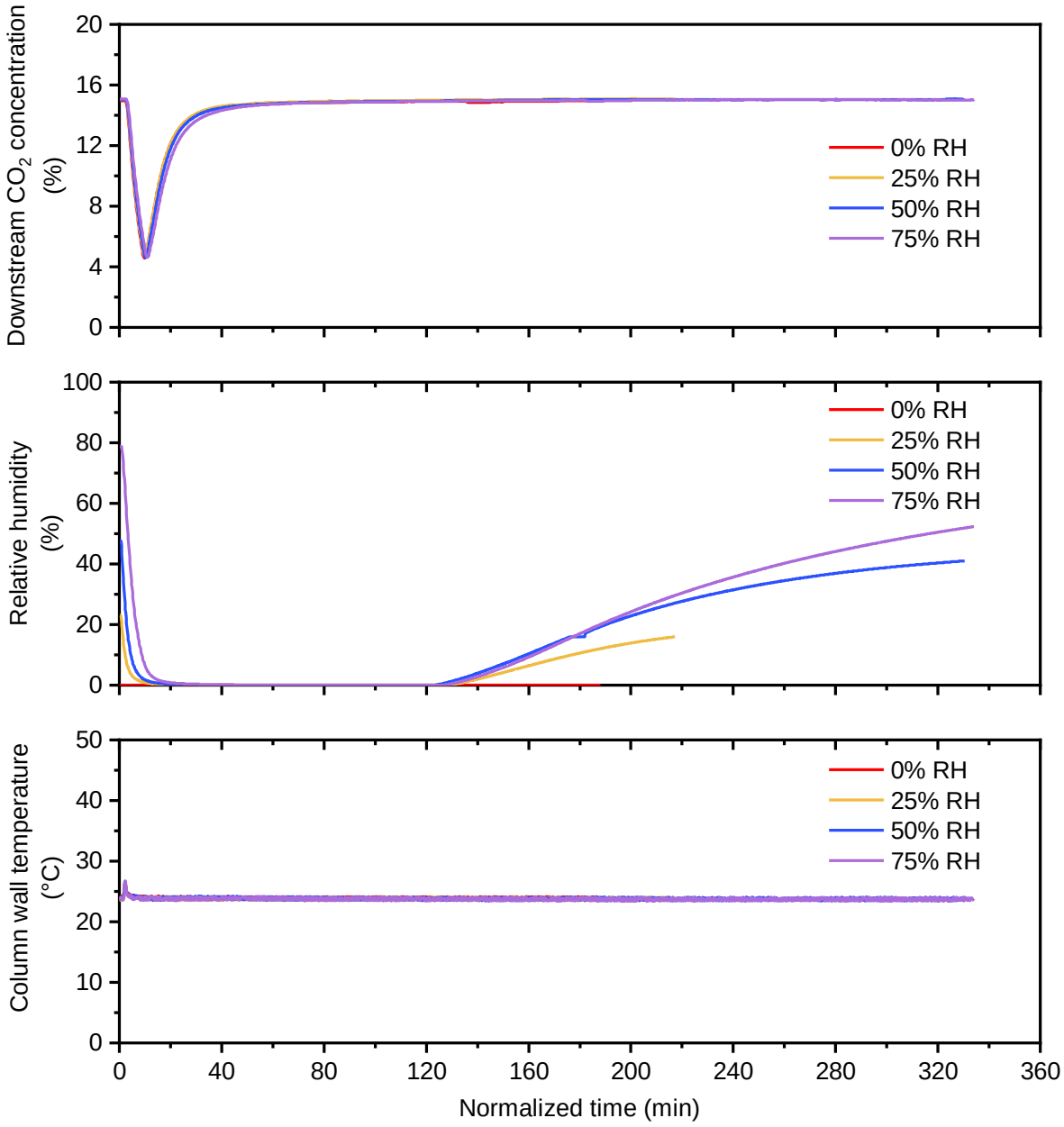

Supplementary Fig. 19 | Dynamic breakthrough measurements of COF-999 at 15% of CO_2 with 0% (red), 25% (yellow), 50% (blue), and 75% (purple) RH at 25°C. 260 mg COF-999 sample and 0.96 cm s^{-1} gas velocity were used in the measurement. The CO_2 uptakes were calculated to be 2.34, 2.48, 2.63, and 3.24 mmol g^{-1}, respectively.

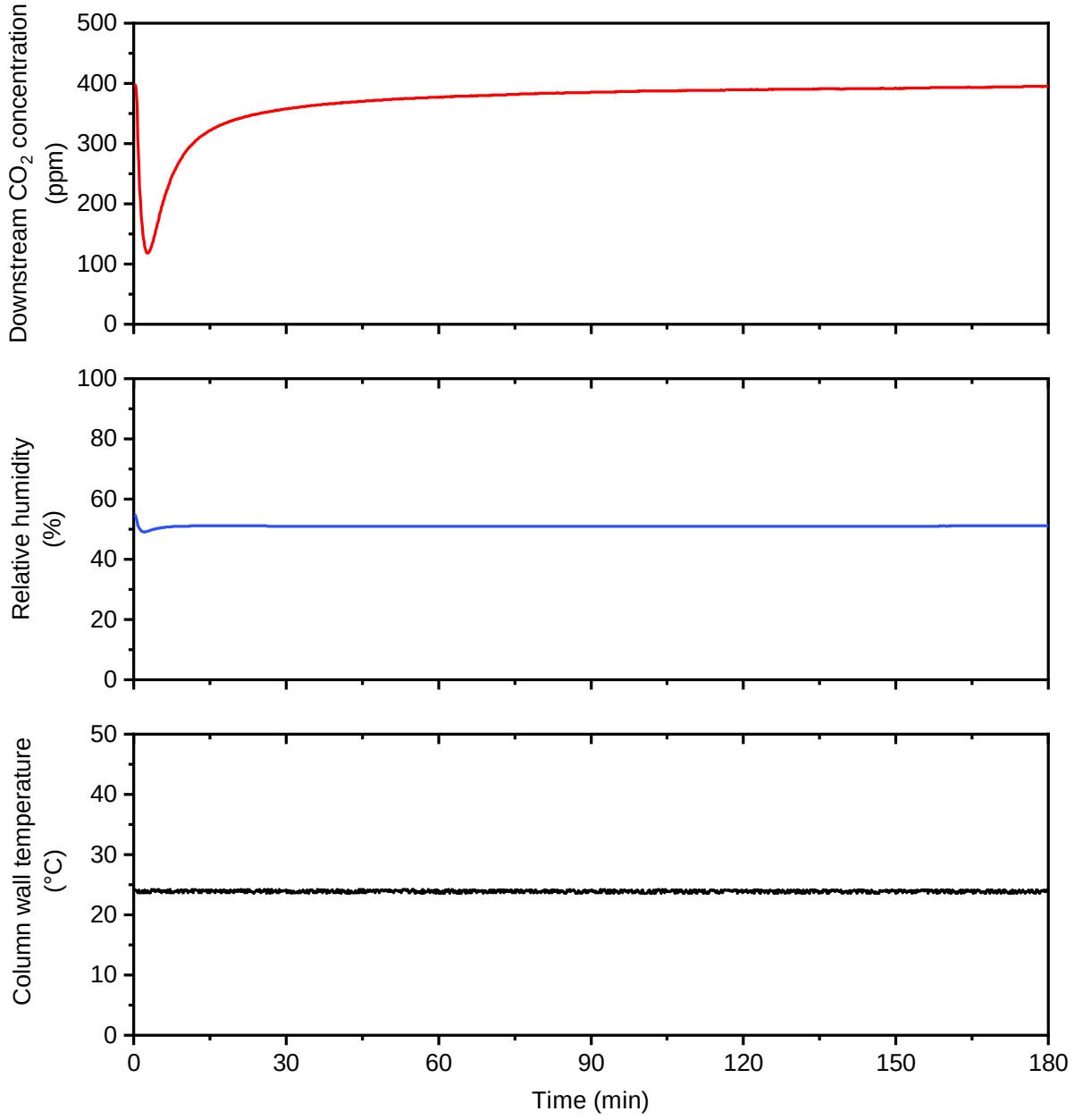

Supplementary Fig. 20 | Adsorption kinetics measurement of COF-999 using simulated air (400 ppm of CO_2 balanced in 4/1 N_2/O_2 with 50% RH) at 25 °C. 5.0 mg COF-999 sample and 4.8 cm s^{-1} gas velocity were used in the measurement. The specific CO_2 uptake of the sample was then obtained as the difference between the apparent and background uptakes per unit mass of the sample.

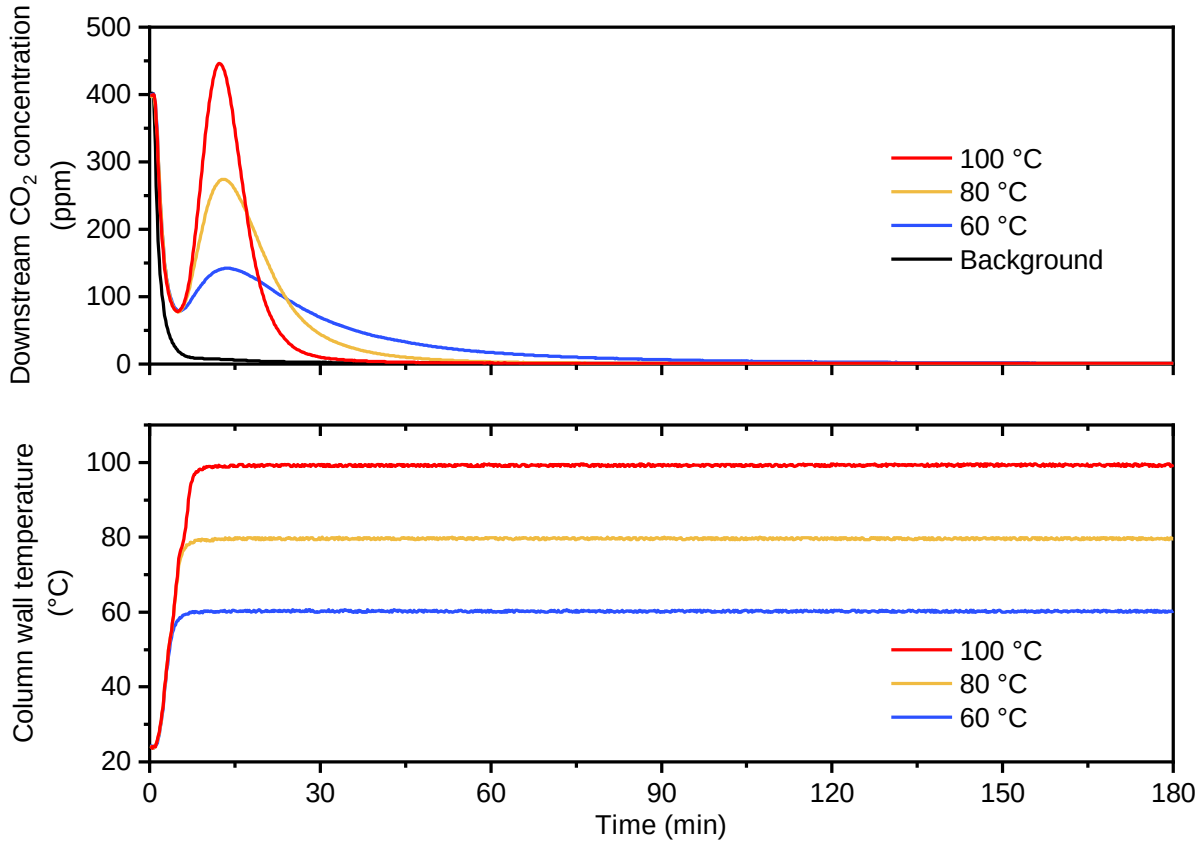

Supplementary Fig. 21 | Desorption kinetics measurements of COF-999 under N_2 flow at 60 °C (blue), 80 °C (yellow), and 100 °C (red). 5.0 mg COF-999 sample and 4.8 cm s^{-1} gas velocity were used in the measurement. The sample was saturated with simulated air (400 ppm of CO_2 balanced in 4/1 N_2/O_2 with 50% RH) before the measurement. The background curve was measured without the sample in the column to eliminate the impact of the remaining CO_2 in the gas line. The amount of desorbed CO_2 was calculated by the integration of downstream CO_2 concentration over time.

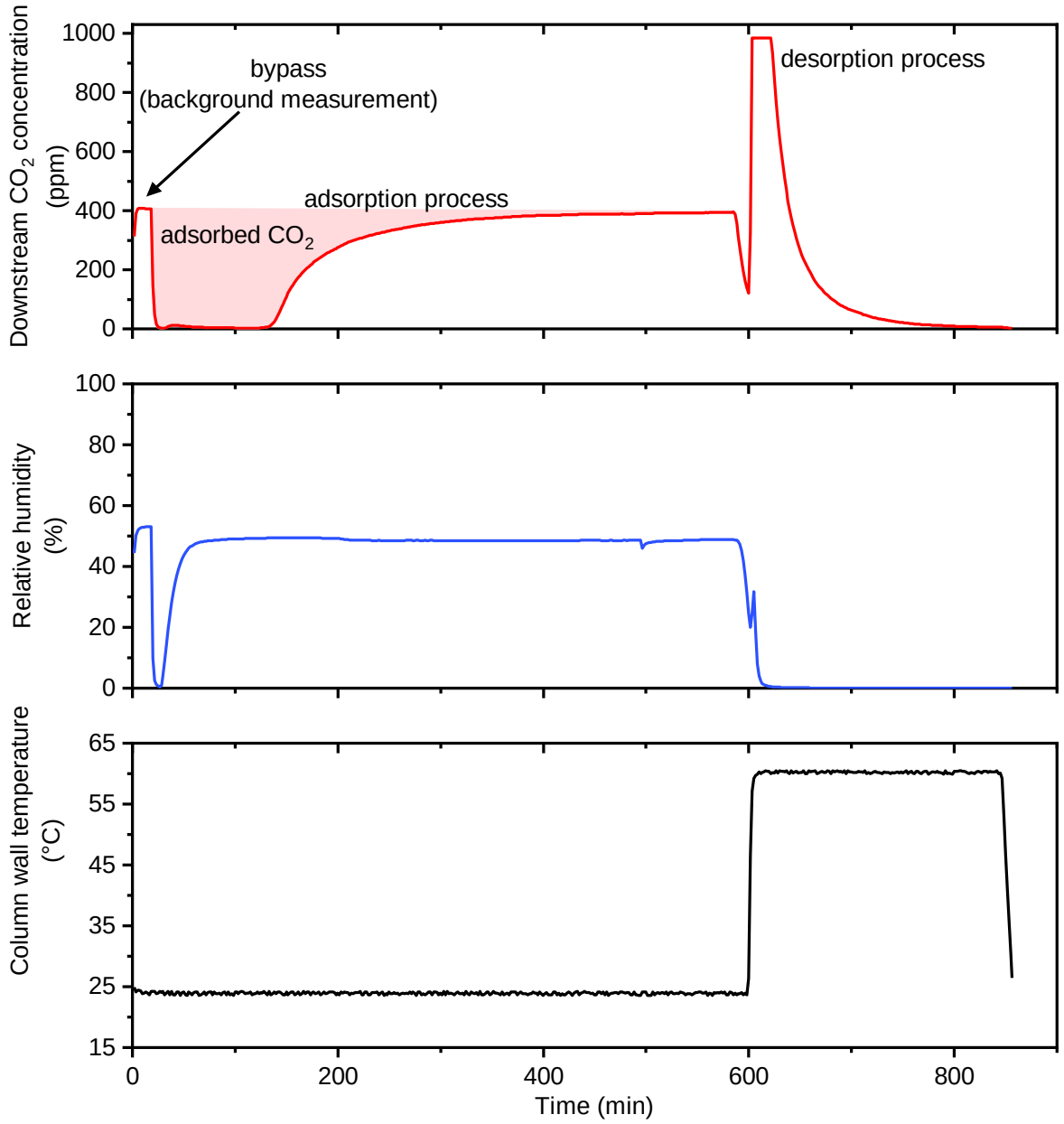

Supplementary Fig. 22 | One temperature-swing CO_2 breakthrough cycle conducted on COF-999. Simulated air (400 ppm of CO_2 balanced in 4/1 N_2/O_2 with 50% RH) was used in the adsorption process. In the plot of the downstream CO_2 concentration, the CO_2 uptake can be derived through numerical integration of the marked area. The detection range of the CO_2 sensor is 0.6 to 984.9 ppm.

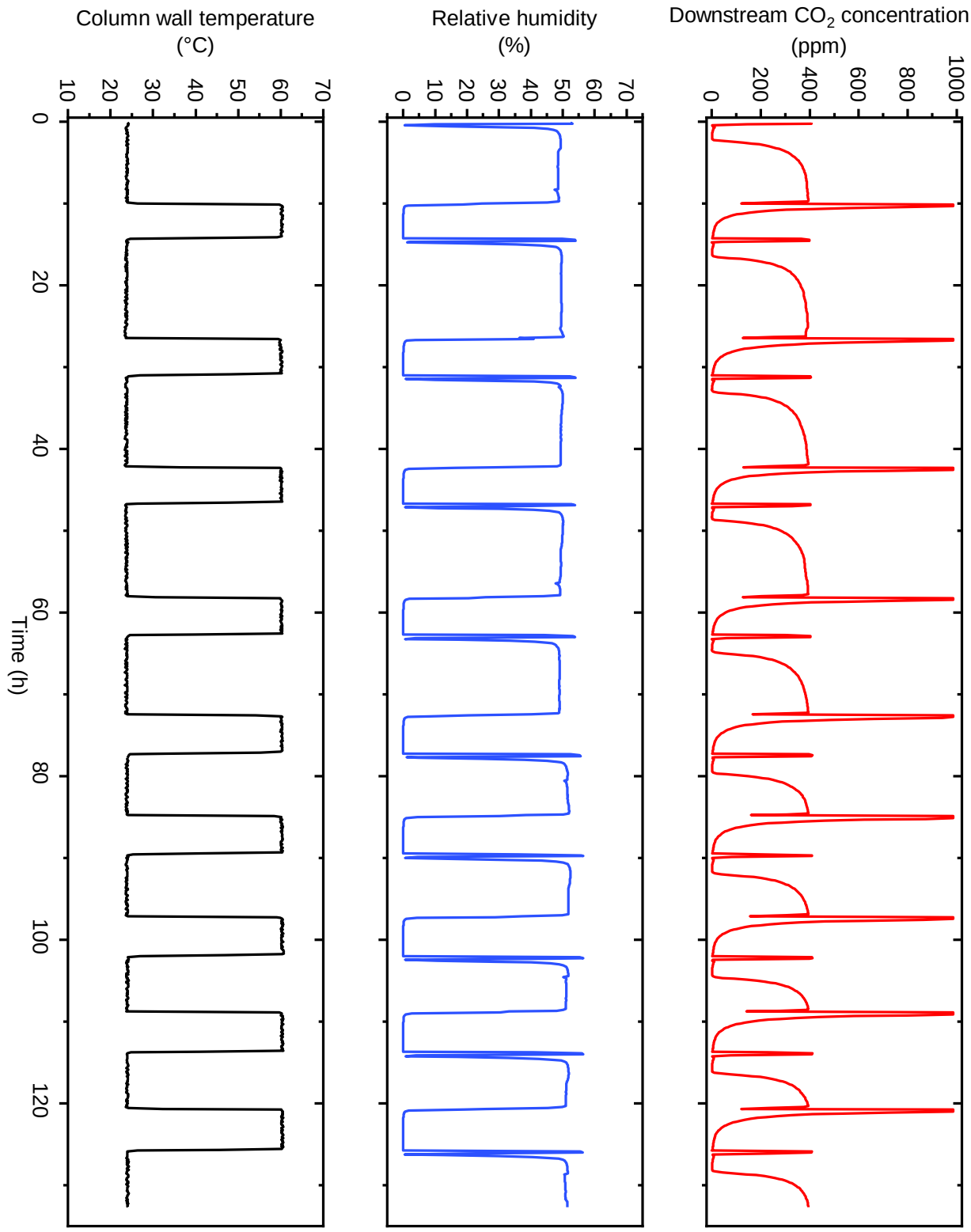

Supplementary Fig. 23 | Ten temperature-swing CO_2 breakthrough cycles conducted on COF-999. Simulated air (400 ppm of CO_2 balanced in 4/1 N_2/O_2 with 50% RH) was used in the adsorption process.

Section 11. CO_2 Breakthrough Experiments Using Open Air

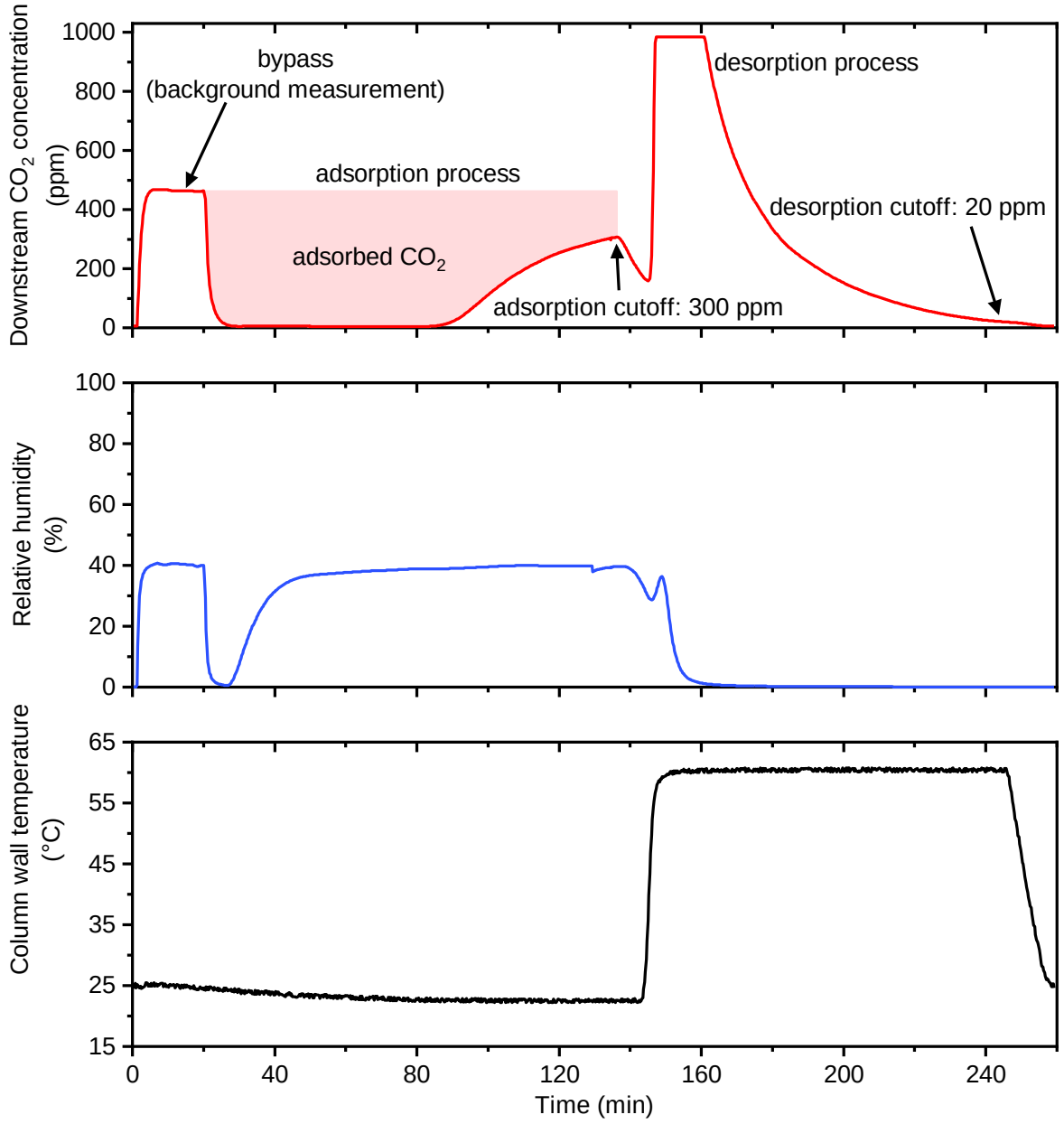

Supplementary Fig. 24 | One temperature-swing CO_2 breakthrough cycle conducted on COF-999 by using outdoor air as the CO_2 source. In the plot of the downstream CO_2 concentration, the CO_2 uptake can be derived through numerical integration of the marked area. The detection range of the CO_2 sensor is 0.6 to 984.9 ppm.

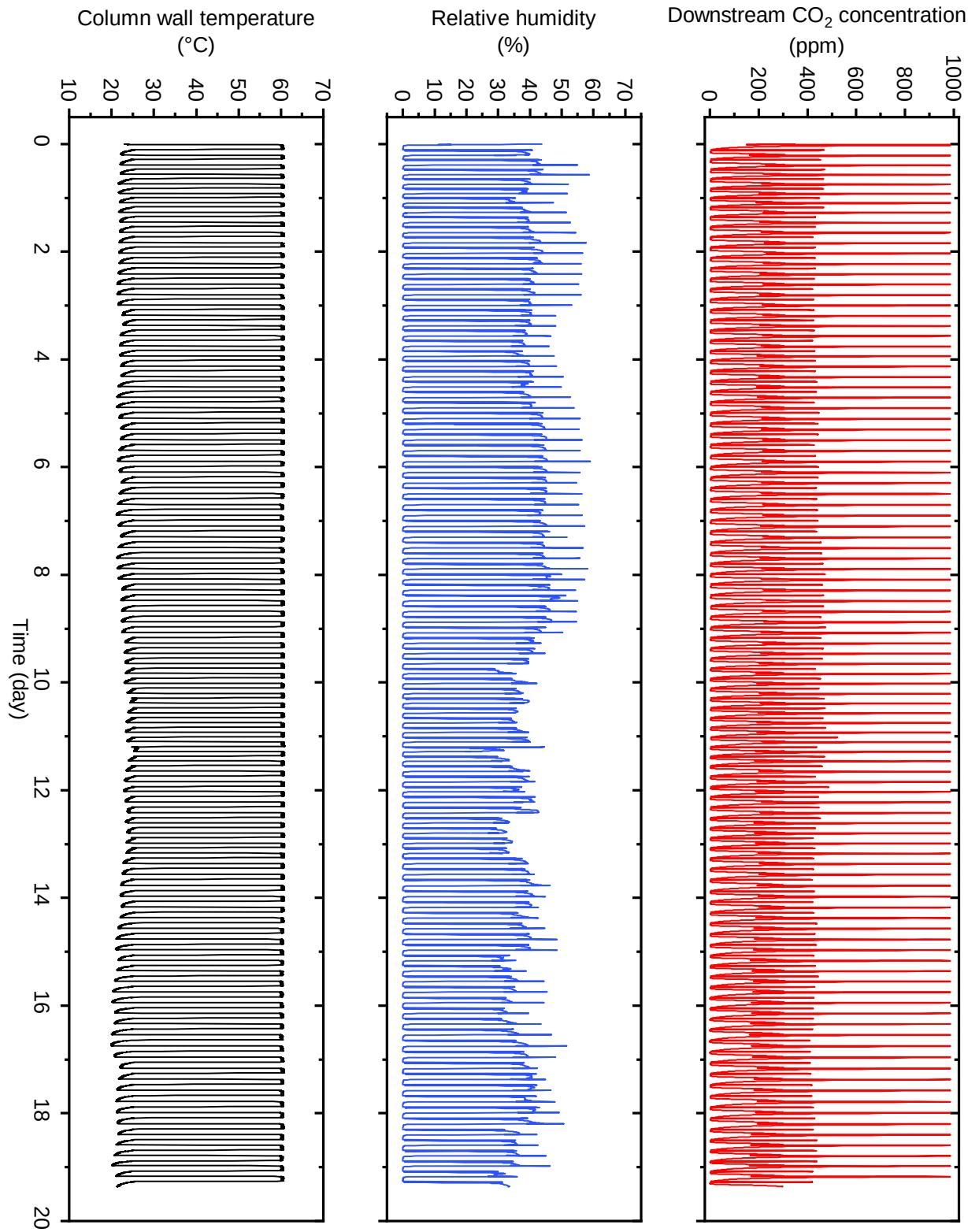

Supplementary Fig. 25 | One hundred temperature-swing CO_2 breakthrough cycles conducted on COF-999 by using outdoor air as the CO_2 source over a 20-day experiment.

Section 12. Desorption energy of COF-999

The isosteric heat of CO_2 adsorption (53 kJ mol^{-1}) under dry conditions and the isosteric heat of water adsorption (49 kJ mol^{-1}) are calculated from the Clausius-Clapeyron equation through CO_2 and water isotherms in Section 5.

Under humid conditions, water-carbamate hydrogen bonding and water desorption are the major contributors to consider in the calculation of energy. In the energy estimation at the laboratory stage, the sorbent's sensible heat (Q_{sens}) and desorption enthalpy (Q_{des}) during the desorption process are primarily considered [33,34]:

$$Q_{sens} = \left(C_{p,CO2} + \frac{q_{H2O}}{q_{CO2}} C_{p,H2O} + \frac{1}{q_{CO2}} C_{p,sorbent}\right) \times (T_{des} - T_{ads})$$

$$Q_{des} = \Delta H_{CO2} + \frac{q_{H2O}}{q_{CO2}} \Delta H_{H2O} + \Delta H_{H-bond}$$

The physical properties used in the calculation are as follows:

Physical properties	Values
Heat capacity of sorbent, $C_{p,sorbent}$	1.5[a] kJ kg^{-1} K^{-1}
Heat capacity of CO_2, $C_{p,CO2}$	0.85 kJ kg^{-1} K^{-1}
Heat capacity of water, $C_{p,H2O}$	4.18 kJ kg^{-1} K^{-1}
Heat of adsorption of CO_2[b], ΔH_{CO2}	53 kJ mol^{-1}
Heat of adsorption of water[b], ΔH_{H2O}	49 kJ mol^{-1}
Heat of hydrogen bond dissociation[c], ΔH_{H-bond}	49 kJ mol^{-1}
$T_{des} - T_{ads}$	35 °C
Water and CO_2 capacity ratio[d], q_{H2O}/q_{CO2}	2.5

a, Estimated from similar structures [35].

b, Isosteric heat of adsorption, calculated from the Clausius-Clapeyron equation (Supplementary Figs. 6 and 8).

c, Estimated from DFT calculation (Section 14), the difference between the CW1 and CA1 energies corresponds to the sum of the total energy to the dissociation of multiple hydrogen bonds.

d, Calculated from water (5.0 mmol g^{-1}) and CO_2 (2.0 mmol g^{-1}) capacities under 400 ppm CO_2 and 50% RH.

From these data, COF-999 requires a total heat of 259 kJ mol^{-1} for desorption under 60 °C after the adsorption from 400 ppm CO_2 and 50% RH (including 34 kJ mol^{-1} sensible heat and 225 kJ mol^{-1} desorption enthalpy). The materials reported in the literature use a desorption temperature of 100 °C or higher instead of the lower temperature of 60 °C needed for desorption in our case. Thus, to make a comparison, we recalculated our energetics at 100 °C, and the comparison of the literature is as follows: the state-of-the-art solid amine sorbents require a sensible heat of 73 kJ mol^{-1}, and a total energy of 298 kJ mol^{-1}. Other reported solid-supported amines are also usually more hydrophilic and take up water to CO_2 in a 4 to 12 ratio[33], leading to a total energy requirement of 336 to 749 kJ mol^{-1} if desorbed under 60 °C. From the calculation, the energy requirements for our material are significantly lower than those of other sorbents.

Overall, the hydrophobic nature of COF-999 results in a lower energy requirement under low desorption temperatures, making it advantageous for future industrial development.

Section 13. Solid-State Nuclear Magnetic Resonance Spectra (ssNMR)

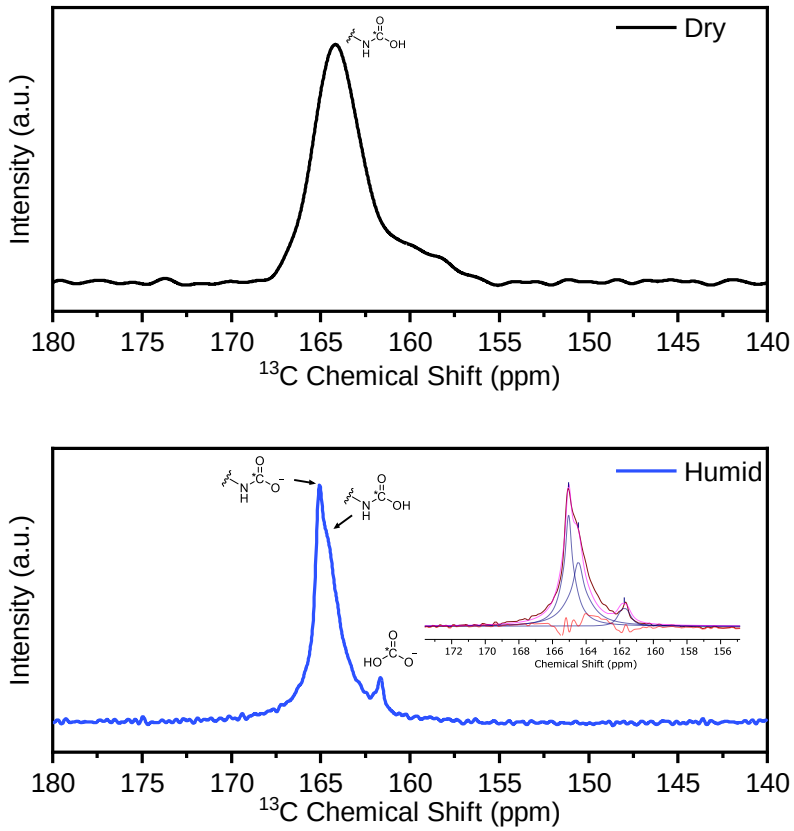

Supplementary Fig. 26 | ^{13}C solid-state NMR spectra of $^{13}CO_2$ dosing experiments performed on COF-999 under dry (black) and humid (blue) conditions. Illustrative schemes of major sorption products are provided to highlight the assignments of signals and chemical conversion of species. Isotopic labeling sites are marked with "*" for ^{13}C. Inset shows the result of linear deconvolution of the overlapping region. Color code for inserted graph: experimental data, brown; simulated peak profiles, blue; sum of simulated signals, violet; simulation-experiment difference, red.

Section 14. Density Functional Theory Calculations (DFT)

DFT calculations were performed to investigate the mechanism of CO_2 adsorption in COF-999 both in the absence and presence of water molecules (dry and humid conditions for CO_2 capture respectively). We note that the polyethyleneimine units can exhibit significant conformational flexibility, which allows the polyamine chains to adjust to favored CO_2 adsorption structures under dry and wet conditions and thus, maximize their CO_2 uptake.

Formation of carbamic acid/carbamate under dry conditions

Under dry conditions, the formation of carbamic acid/carbamate (Supplementary Table 7, CA1-CA3) upon the reaction of the CO_2 molecules with the polyamine groups is energy-favorable (ΔE = –75 to –101 kJ·mol^{-1}). Carbamic acid is stabilized through H-bond interactions with adjacent polyamine groups (N···O distances about 263-273 pm). Carbamates are thermodynamically favored over adsorbed CO_2 molecules under dry conditions.

Supplementary Table 7 | Zoomed-in view of optimized structures of carbamic acid/carbamates in the absence of water molecules formed during CO_2 adsorption in COF-999 and the corresponding reaction energies, ΔE (kJ·mol^{-1}). The hydrogen bond distances between O_{CO2} and N_{amine} as well as the corresponding O-H and N_{amine}-H distances (within square brackets) are given in *pm*.

	CA1	**CA2**	**CA3**
	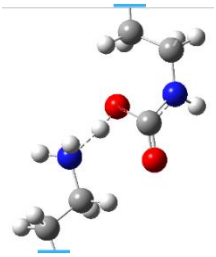	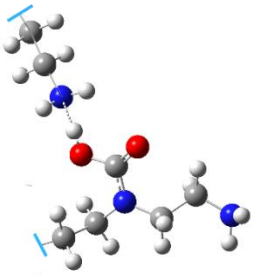	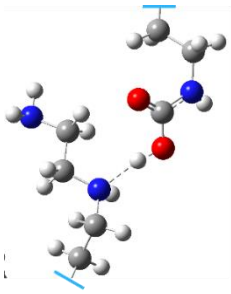
ΔE	-101.3	-75.5	-74.7
O···N [O-H/N-H]	263 [105 / 159]	263 [104 / 159]	273 [102 / 176]

Formation of carbamic acid/carbamate under humid conditions

Under humid conditions, carbamic acid/carbamate (Supplementary Table 8, CW1-CW3) formed upon the reaction of CO_2 molecules with polyamines are stabilized through hydrogen bond interactions with the water molecules (ΔE about –150 kJ·mol^{-1}). The carbamates form hydrogen bonds each with an adjacent polyamine group (N···O[donor] distances about 257-262 pm and N[donor]···O distances about 281-317 pm) and a water molecule (O···O_{water} distances about 266-283 pm). The proton is delocalized between the oxygen atom of carbamate and the adjacent polyamine group (O···H distances about 105-112 pm and N···H distances about 103-106 pm). The formation of carbamates under humid conditions is thermodynamically more favorable than the formation of bicarbonates under humid conditions.

Supplementary Table 8 | Zoomed-in view of optimized structures of carbamic acid/carbamates in the presence of water molecules formed during CO_2 adsorption in COF-999 and the corresponding reaction energies, ΔE (kJ·mol^{-1}). The hydrogen bond distances between O_{CO2} and N_{amine} as well as the corresponding O-H and N_{amine}-H distances (within square brackets) are given in *pm*.

	CW1	**CW2**	**CW3**
	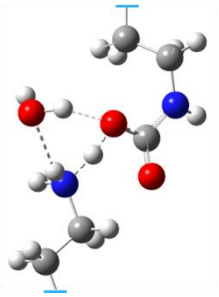	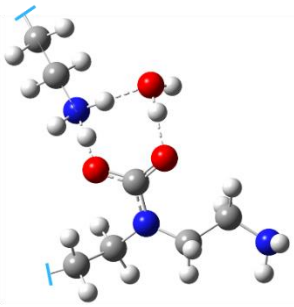	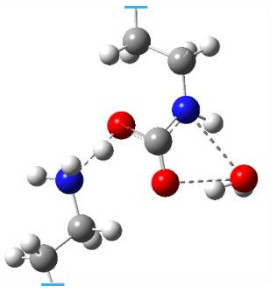
ΔE	-150.0	-149.2	-149.0
O···N	257 [110 / 145]	259 [112 / 147]	262 [105 / 158]
[O-H/N-H]	317 [238 / 103]	281 [175 / 106]	286 [195 / 103]
	283 [187 / 99]	266 [164 / 102]	275 [184 / 99]

Formation of carbonic acid/bicarbonate under humid conditions

Under humid conditions, a CO_2 molecule can form carbonic acid/bicarbonate (Supplementary Table 9, BC1-BC3) upon reaction with a water molecule assisted by the polyamine group (ΔE = –82 to –110 kJ·mol^{-1}). The bicarbonates form at least one strong hydrogen bond with the polyamine groups (N···O distances about 254-263 pm) and are further stabilized through up to two additional hydrogen bonds with the adjacent polyamines (N···O distances about 271-334 pm). The bicarbonates donate up to two hydrogen bonds to the polyamines through its -OH groups and accept one hydrogen bond through its =O group. The proton is delocalized between the oxygen atom of bicarbonate and the polyamine group (O···H distances about 103-111 pm and N···H distances about 103-107 pm).

Supplementary Table 9 | Zoomed-in view of optimized structures of carbonic acid/bicarbonates in the absence of water molecules formed during CO_2 adsorption in COF-999 and the corresponding reaction energies, ΔE (kJ·mol^{-1}). The hydrogen bond distances between O_{CO2} and N_{amine} as well as the corresponding O-H and N_{amine}-H distances (within square brackets) are given in *pm*.

	BC1	**BC2**	**BC3**
	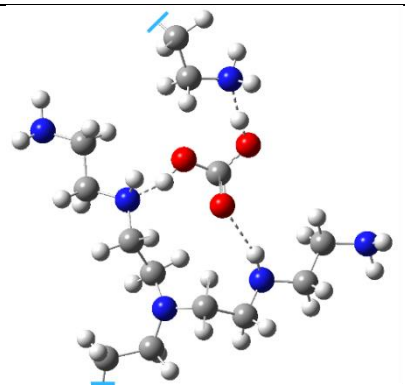	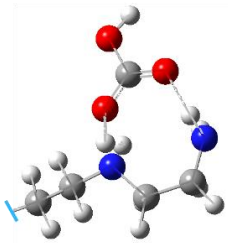	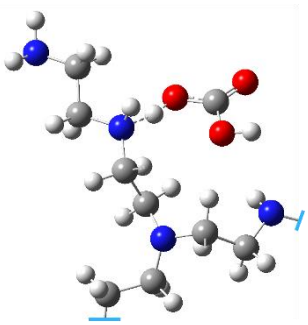
ΔE	-110.4	-85.3	-81.9
O···N [O-H/N-H]	262 [105 / 163], 271 [103 / 168], 319 [220 / 103]	263 [168 / 107], 298 [195 / 103], 328 [233 / 103]	254 [111 / 144], 334 [246 / 103]

Supplementary Table 10 | Absolute electronic energies (in eV) and relative electronic energies (kJ·mol^{-1}) of different intermediates formed upon CO_2 adsorption.

Structure	n_{CO_2}	n_{H_2O}	$E_{\text{empty COF}}$	$E_{\text{ads,system}}$	ΔE
	-	-	eV	eV	kJ·mol^{-1}
iso. CO_2	1	-	-	-23.015565	-
iso. H_2O	-	1	-	-14.368719	-
CA1	1	0	-2306.698192	-2330.763490	–101.3
CA2	1	0	-2307.218053	-2331.016320	–75.5
CA3	1	0	-2306.698192	-2330.487753	–74.7
CW1	1	1	-2306.698192	-2345.638642	–150.0
CW2	1	1	-2307.218053	-2346.148992	–149.2
CW3	1	1	-2306.698192	-2345.626718	–149.0
BC1	1	1	-2306.698192	-2345.226623	–110.4
BC2	1	1	-2307.218053	-2345.486146	–85.3
BC3	1	1	-2306.698192	-2344.931325	–81.9

Section 15. Solution-State Nuclear Magnetic Resonance Spectra (Solution-State NMR)

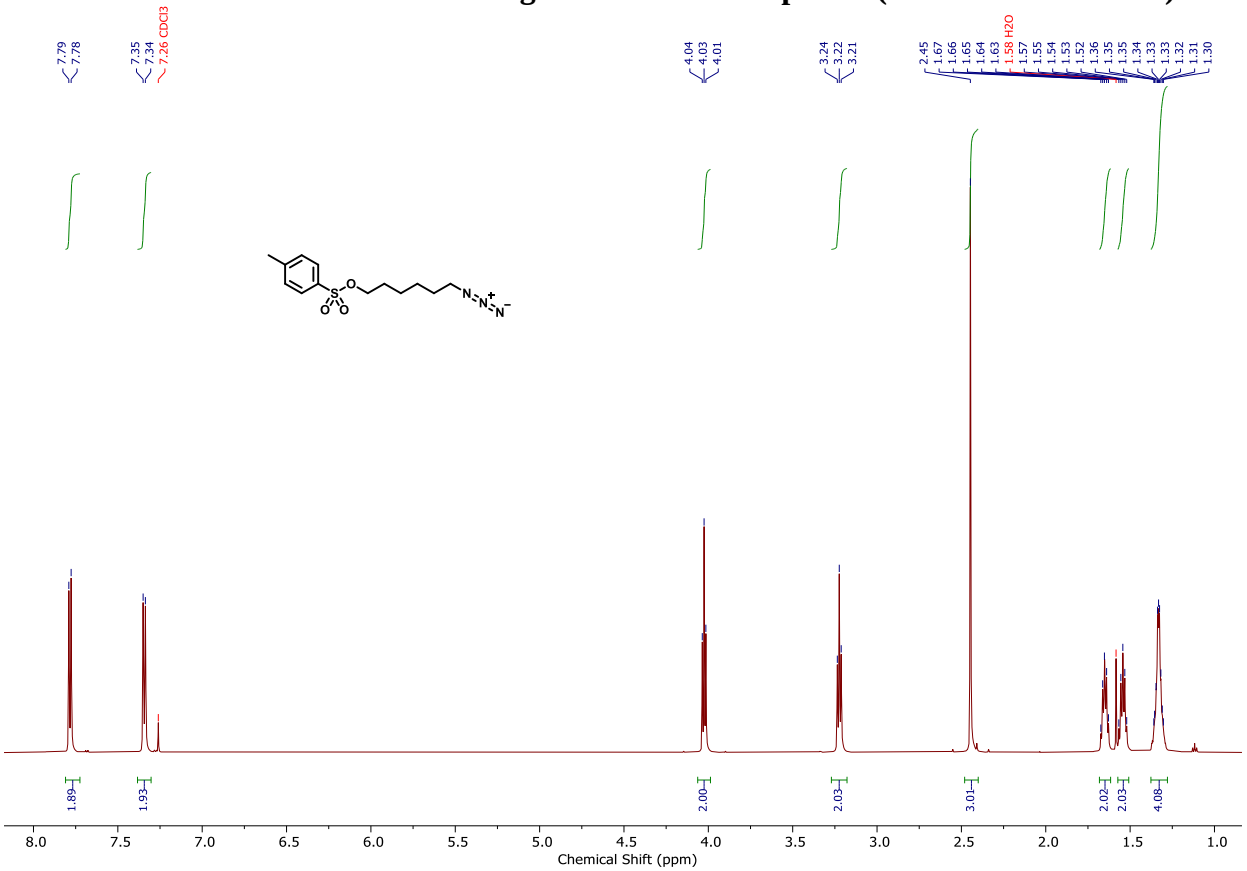

Supplementary Fig. 27 | ^{1}H NMR (600 MHz) spectrum of 1-hexanol, 6-azido-, 1-(4-methylbenzenesulfonate) in $CDCl_3$.

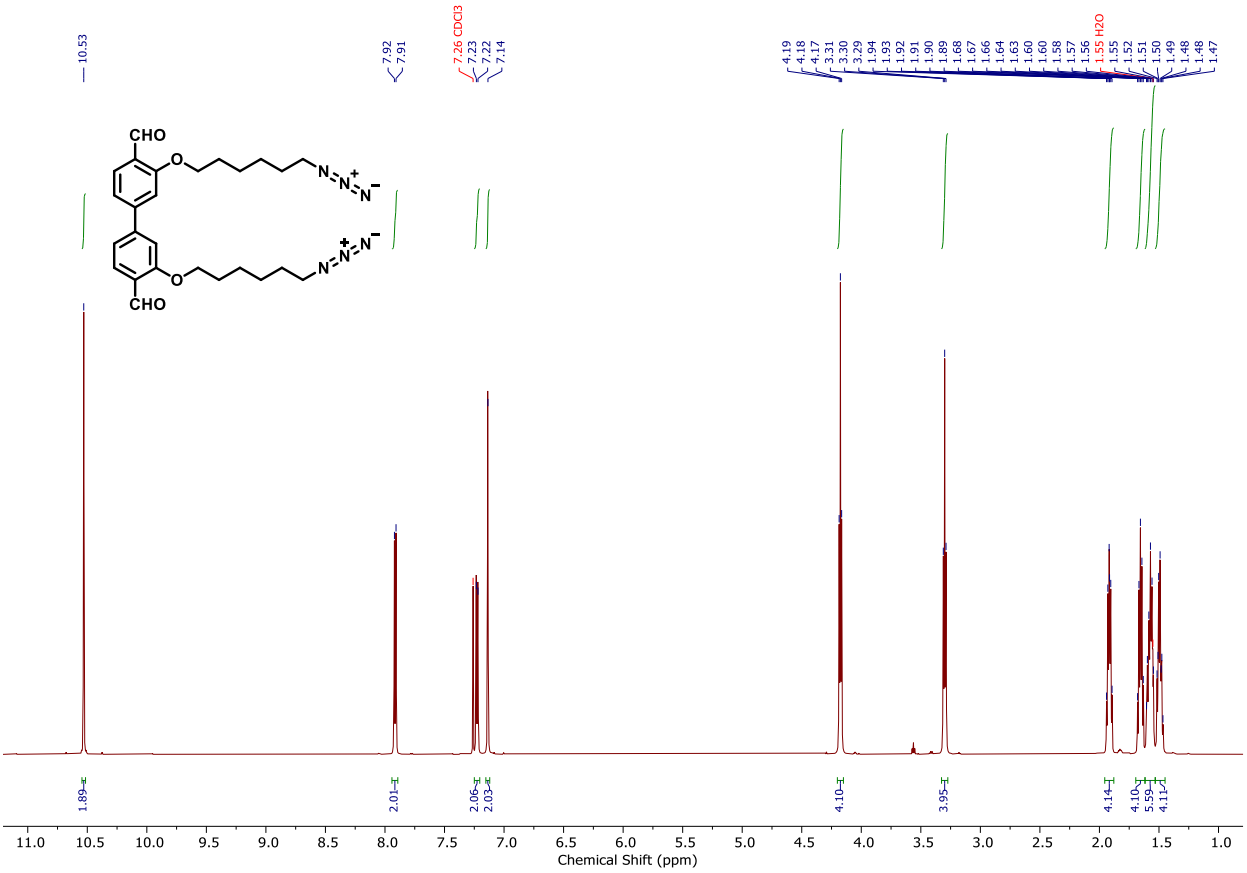

Supplementary Fig. 28 | ^{1}H NMR (600 MHz) spectrum of BPDA-N_3 in $CDCl_3$.

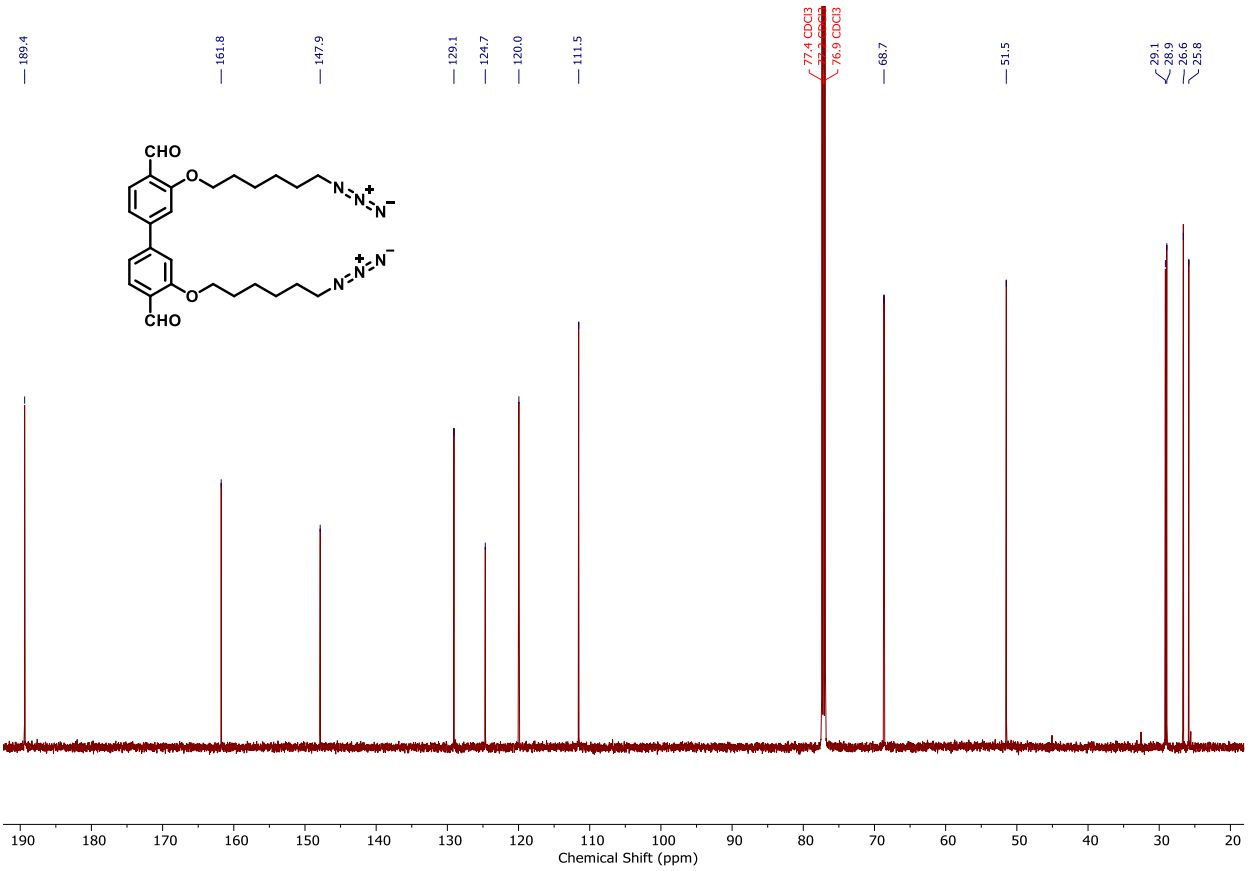

Supplementary Fig. 29 | ^{13}C NMR (151 MHz) spectrum of BPDA-N_3 in $CDCl_3$.

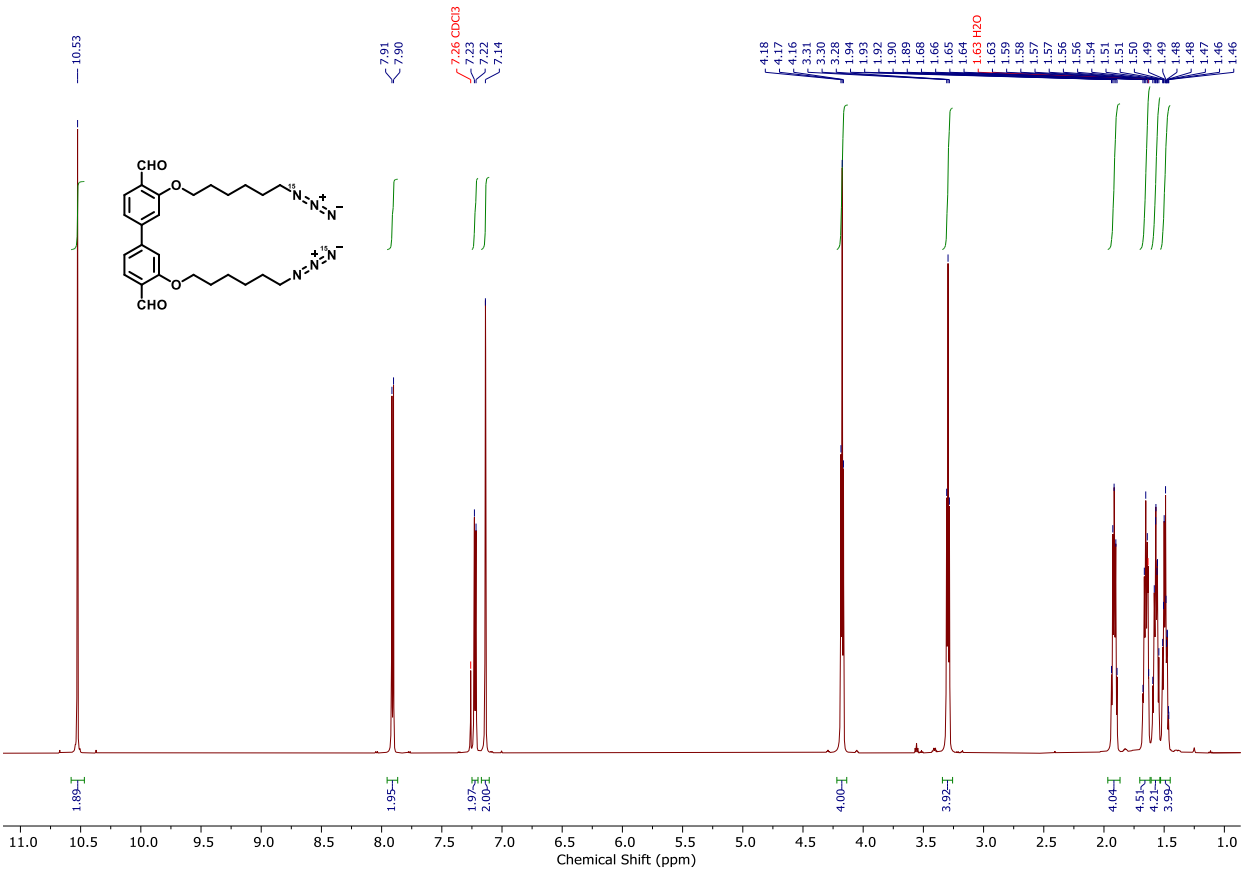

Supplementary Fig. 30 | ^{1}H NMR (600 MHz) spectrum of BPDA-$^{15}NN_2$ in $CDCl_3$. BPDA-$^{15}NN_2$ is a mixture of α-^{15}N (R–^{15}N=N=N) and γ-^{15}N (R–N=N=^{15}N) labeled compounds.

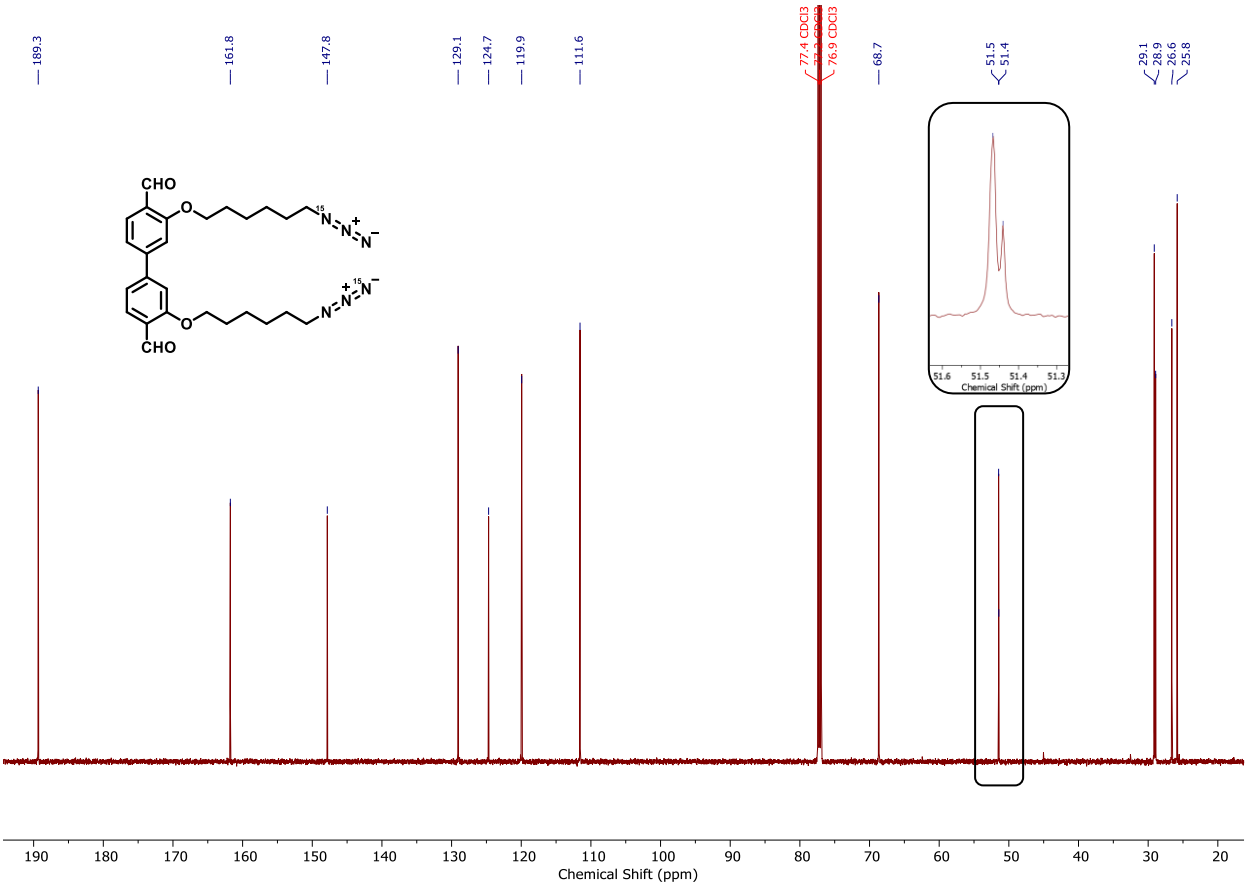

Supplementary Fig. 31 | ^{13}C NMR (151 MHz) spectrum of BPDA-$^{15}NN_2$ in $CDCl_3$. BPDA-$^{15}NN_2$ is a mixture of α-^{15}N (R–^{15}N=N=N) and γ-^{15}N (R–N=N=^{15}N) labeled compounds. The chemical shift ranging from 51.6 to 51.3 ppm is magnified.

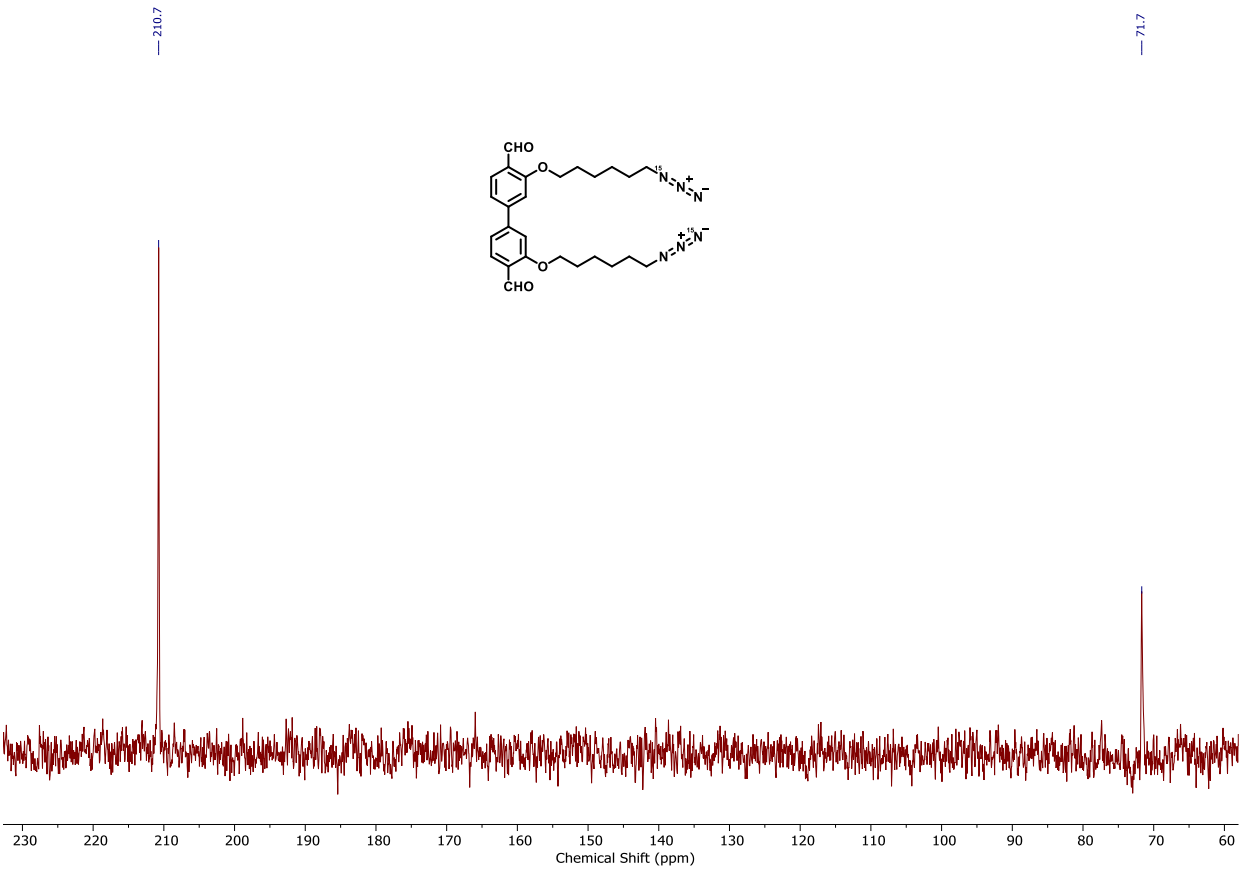

Supplementary Fig. 32 | ^{15}N NMR (61 MHz) spectrum of BPDA-$^{15}NN_2$ in $CDCl_3$. BPDA-$^{15}NN_2$ is a mixture of α-^{15}N (R–^{15}N=N=N) and γ-^{15}N (R–N=N=^{15}N) labeled compounds.

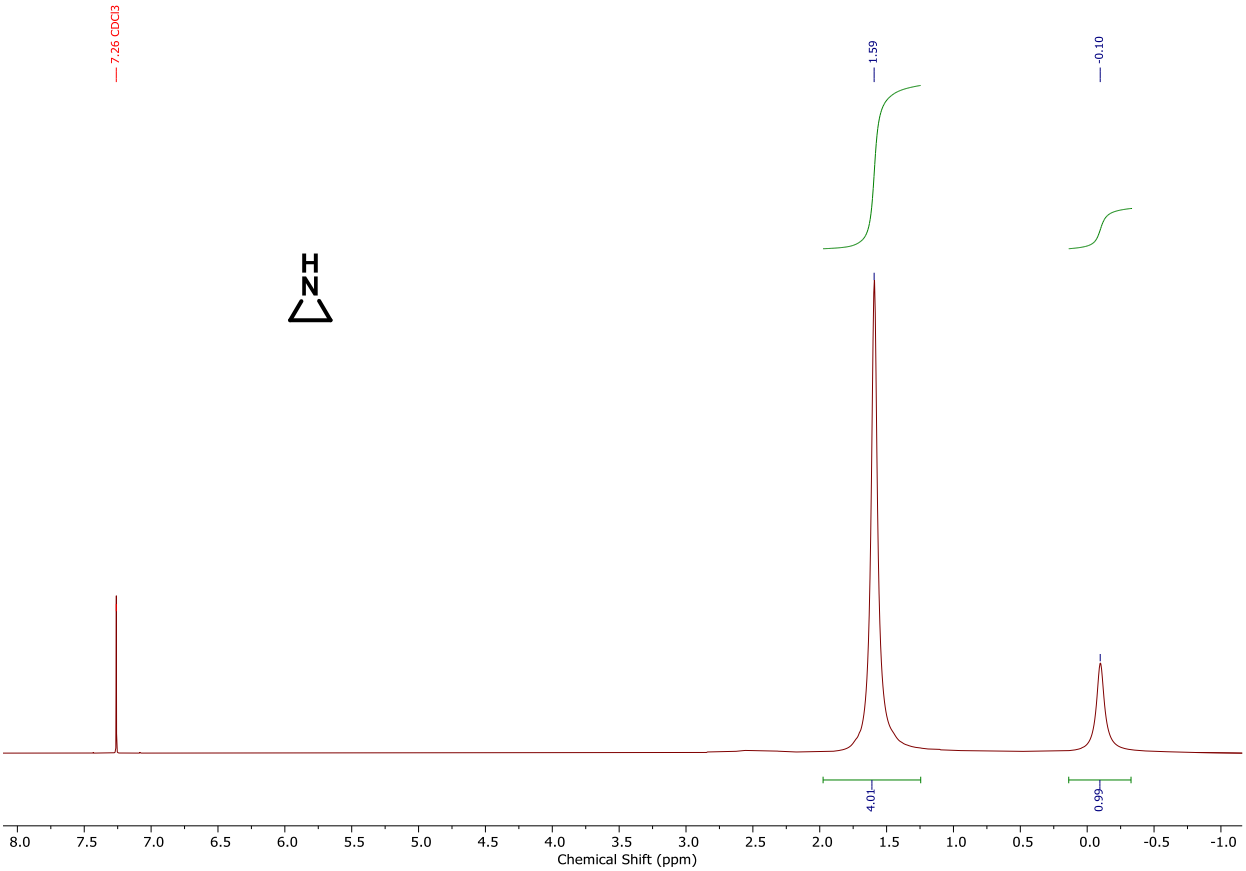

Supplementary Fig. 33 | ^{1}H NMR (600 MHz) spectrum of aziridine in $CDCl_3$.

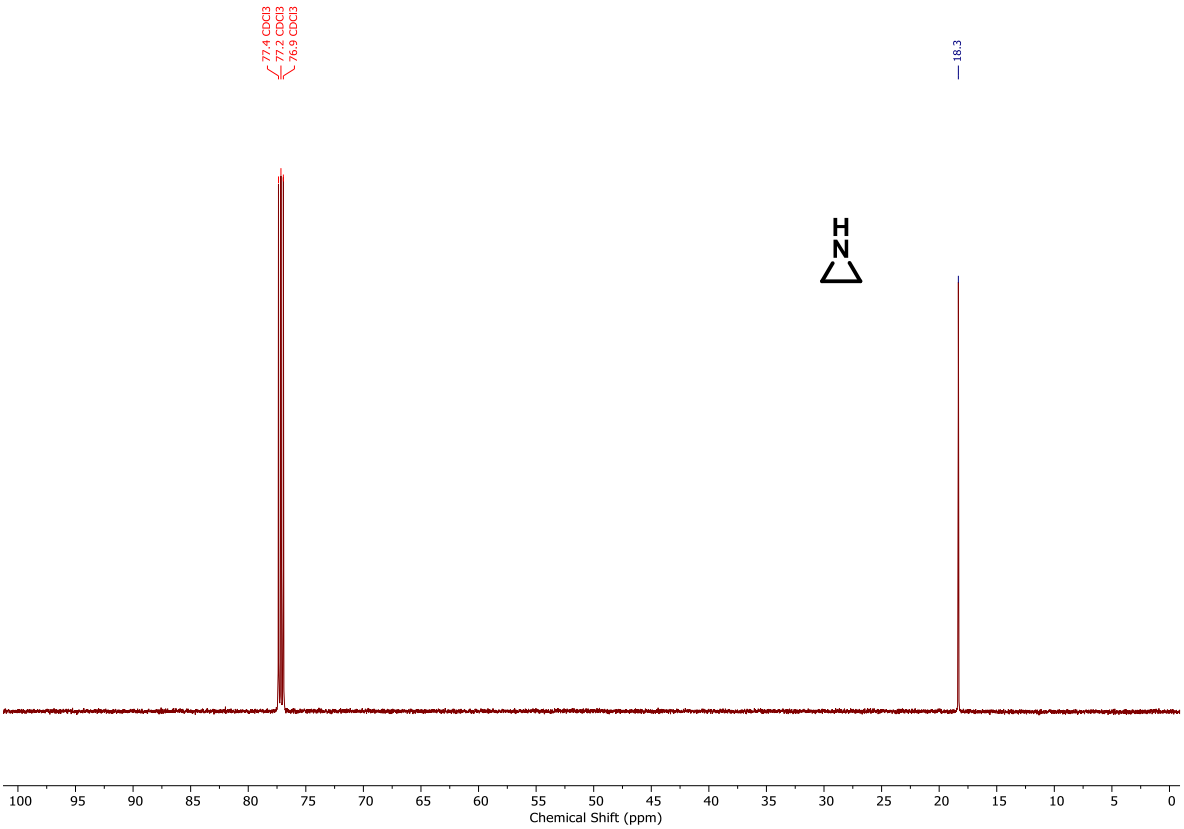

Supplementary Fig. 34 | ^{13}C NMR (151 MHz) spectrum of aziridine in $CDCl_3$.

References

1. Lyu, H., Li, H., Hanikel, N., Wang, K. & Yaghi, O. M. Covalent organic frameworks for carbon dioxide capture from air. *J. Am. Chem. Soc.* **144**, 12989–12995 (2022).
2. Zhang, X. *et al.* Direct air capture of CO_2 in designed metal-organic frameworks at lab and pilot scale. *Carbon Capture Sci. Technol.* **9**, 100145 (2023).
3. Shekhah, O. *et al.* Made-to-order metal-organic frameworks for trace carbon dioxide removal and air capture. *Nat. Commun.* **5**, 4228 (2014).
4. McDonald, T. M. *et al.* Capture of carbon dioxide from air and flue gas in the alkylamine-appended metal–organic framework mmen-Mg_2 (dobpdc). *J. Am. Chem. Soc.* **134**, 7056–7065 (2012).
5. Choi, S., Watanabe, T., Bae, T.-H., Sholl, D. S. & Jones, C. W. Modification of the Mg/DOBDC MOF with amines to enhance CO_2 adsorption from ultradilute gases. *J. Phys. Chem. Lett.* **3**, 1136–1141 (2012).
6. Bien, C. E. *et al.* Bioinspired metal–organic framework for trace CO_2 capture. *J. Am. Chem. Soc.* **140**, 12662–12666 (2018).
7. Chen, O. I.-F. *et al.* Water-enhanced direct air capture of carbon dioxide in metal-organic frameworks. *J. Am. Chem. Soc.* **146**, 2835–2844 (2024).
8. Zhu, X. *et al.* Recent advances in direct air capture by adsorption. *Che. Soc. Rev.* **51**, 6574–6651 (2022).
9. Kwon, H. T. *et al.* Aminopolymer-impregnated hierarchical silica structures: unexpected equivalent CO_2 uptake under simulated air capture and flue gas capture conditions. *Chem. Mater.* **31**, 5229–5237 (2019).
10. Miao, Y., He, Z., Zhu, X., Izikowitz, D. & Li, J. Operating temperatures affect direct air capture of CO_2 in polyamine-loaded mesoporous silica. *Chem. Eng. J.* **426**, 131875 (2021).
12. Zhu, X. *et al.* Efficient CO_2 capture from ambient air with amine-functionalized Mg–Al mixed metal oxides. *J. Mater. Chem. A* **8**, 16421–16428 (2020).
12. Wang, J. *et al.* Direct capture of low-concentration CO_2 on mesoporous carbon-supported solid amine adsorbents at ambient temperature. *Ind. Eng. Chem. Res.* **54**, 5319–5327 (2015).
13. Kong, Y., Jiang, G., Wu, Y., Cui, S. & Shen, X. Amine hybrid aerogel for high-efficiency CO_2 capture: effect of amine loading and CO_2 concentration. *Chem. Eng. J.* **306**, 362–368 (2016).
14. Kumar, D. R. *et al.* Alkyl-aryl amine-rich molecules for CO_2 removal via direct air capture. *ACS Sustain. Chem. Eng.* **8**, 10971–10982 (2020).
15. Rosu, C. *et al.* Effect of extended aging and oxidation on linear poly(propylenimine)-mesoporous silica composites for CO_2 capture from simulated air and flue gas streams. *ACS Appl. Mater. Interfaces* **12**, 38085–38097 (2020).
16. Liu, L., Chen, J., Tao, L., Li, H. & Yang, Q. Aminopolymer confined in ethane-silica nanotubes for CO_2 capture from ambient air. *ChemNanoMat* **6**, 1096–1103 (2020).
17. Sakwa-Novak, M. A., Yoo, C., Tan, S., Rashidi, F. & Jones, C. W. Poly(ethylenimine)-functionalized monolithic alumina honeycomb adsorbents for CO_2 capture from air. *ChemSusChem* **9**, 1859–1868 (2016).
18. Kuwahara, Y. *et al.* Enhanced CO_2 adsorption over polymeric amines supported on heteroatom-incorporated SBA-15 silica: impact of heteroatom type and loading on sorbent structure and adsorption performance. *Chem. Eur. J.* **18**, 16649–16664 (2012).

19. Chaikittisilp, W., Lunn, J. D., Shantz, D. F. & Jones, C. W. Poly(L-lysine) brush–mesoporous silica hybrid material as a biomolecule-based adsorbent for CO_2 capture from simulated flue gas and air. *Chem. Eur. J.* **17**, 10556–10561 (2011).
20. Lackner, K. S. Capture of carbon dioxide from ambient air. *Eur. Phys. J. Special Topics* **176**, 93–106 (2009).
21. He, H. *et al.* Reversible CO_2 capture with porous polymers using the humidity swing. *Energy Environ. Sci.* **6**, 488–493 (2013).
22. Wang, T., Lackner, K. S. & Wright, A. Moisture swing sorbent for carbon dioxide capture from ambient air. *Environ. Sci. Technol.* **45**, 6670–6675 (2011).
23. He, H. *et al.* Porous polymers prepared via high internal phase emulsion polymerization for reversible CO_2 capture. *Polymer* **55**, 385–394 (2014).
24. Zhu, Y., Booth, A. & Hatzell, K. B. Confinement effects on moisture-swing direct air capture. *Environ. Sci. Technol. Lett.* **11**, 89–94 (2024).
25. Song, J. *et al.* Quaternized chitosan/PVA aerogels for reversible CO_2 capture from ambient air. *Ind. Eng. Chem. Res.* **57**, 4941–4948 (2018).
26. Li, H. *et al.* Capturing carbon dioxide from air with charged-sorbents. *Nature* **630**, 654–659 (2024).
27. Kiani, A., Jiang, K. & Feron, P. Techno-economic assessment for CO_2 capture from air using a conventional liquid-based absorption process. *Front. Energy Res.* **8**, (2020).
28. Sanz-Pérez, E. S., Murdock, C. R., Didas, S. A. & Jones, C. W. Direct capture of CO_2 from ambient air. *Chem. Rev.* **116**, 11840–11876 (2016).
29. Bouaboula, H., Chaouki, J., Belmabkhout, Y. & Zaabout, A. Comparative review of direct air capture technologies: from technical, commercial, economic, and environmental aspects. *Chem. Eng. J.* **484**, 149411 (2024).
30. Evans, A. M. *et al.* Trends in the thermal stability of two-dimensional covalent organic frameworks. *Faraday Discuss.* **225**, 226–240 (2021).
31. He, Y. *et al.* One-step fabrication of PEI-modified GO particles for CO_2 capture. *Appl. Phys. A* **125**, 160 (2019).
32. Johnson, R. L. & Schmidt-Rohr, K. Quantitative solid-state ^{13}C NMR with signal enhancement by multiple cross polarization. *J. Magn. Reson.* **239**, 44–49 (2014).
33. Min, Y. J., Ganesan, A., Realff, M. J. & Jones, C. W. Direct air capture of CO_2 using poly(ethyleneimine)-functionalized expanded poly(tetrafluoroethylene)/silica composite structured sorbents. *ACS Appl. Mater. Interfaces.* **14**, 40992–41002 (2022).
34. Wurzbacher, J. A., Gebald, C., Piatkowski, N. & Steinfeld, A. Concurrent separation of CO_2 and H_2O from air by a temperature-vacuum swing adsorption/desorption cycle. *Environ. Sci. Technol.* **46**, 9191–9198 (2012).
35. Mark, J. E. *Physical Properties of Polymers Handbook*. (Springer New York, 2007). doi:10.1007/978-0-387-69002-5.